AD NUMBER

AD481418

NEW LIMITATION CHANGE

TO

Approved for public release, distribution unlimited

FROM

Distribution authorized to U.S. Gov't. agencies and their contractors; Administrative/Operational use; 1966. Other requests shall be referred to Air Force Materials Lab, Wright-Patterson AFB OH 45433.

AUTHORITY

AFML ltr 31 Jul 1972

HEAT TRANSFER IN STRUCTURAL HONEYCOMB COMPOSITES AT HIGH TEMPERATURE

MERRILL L. MINGES

TECHNICAL REPORT AFML-TR-65-233

JANUARY 1966

AIR FORCE MATERIALS LABORATORY
RESEARCH AND TECHNOLOGY DIVISION
AIR FORCE SYSTEMS COMMAND
WRIGHT-PATTERSON AIR FORCE BASE, OHIO

NOTICES

When Government drawings, specifications, or other data are used for any purpose other than in connection with a definitely related Government procurement operation, the United States Government thereby incurs no responsibility nor any obligation whatsoever; and the fact that the Government may have formulated, furnished, or in any way supplied the said drawings, specifications, or other data, is not to be regarded by implication or otherwise as in any manner licensing the holder or any other person or corporation, or conveying any rights or permission to manufacture, use, or sell any patented invention that may in any way be related thereto.

Copies of this report should not be returned to the Research and Technology Division unless return is required by security considerations, contractual obligations, or notice on a specific document.

HEAT TRANSFER IN STRUCTURAL HONEYCOMB
COMPOSITES AT HIGH TEMPERATURE

MERRILL L. MINGES

FOREWORD

This report was prepared by the Materials Engineering Branch, Materials Applications Division of the Air Force Materials Laboratory under Project No. 7381, "Materials Applications," Task No. 738106, "Design Information Development." The work was administered under the direction of the Air Force Materials Laboratory, Research and Technology Division, Wright-Patterson Air Force Base, Ohio. Mr. M. L. Minges was the project manager.

This report covers work accomplished between December 1963 and December 1964. The manuscript of this report was released by the author July 1965 for publication as an RTD Technical Report.

The efforts of Mr. O. J. Zavakos in assisting with the experimental thermal conductance measurements are greatly appreciated as is the work of Mr. D. F. Stevision on the spectral emittance measurements of the L-605 cobalt alloy specimens.

This technical report has been reviewed and is approved.

W. P. CONRARDY, Chief
Materials Engineering Branch
Materials Applications Division
Air Force Materials Laboratory

ABSTRACT

The use of superalloy and refractory alloy honeycomb composites for heat shield and structural components in re-entry vehicle applications is outlined followed by a detailed comparison between experimentally measured and analytically predicted thermal conductance values on superalloy honeycomb composites.

The experimental thermal conductance determinations on L-605 cobalt alloy panels of variable geometry were made in high vacuum and air environments using a high temperature absolute thermal conductivity apparatus. Measurements were made over the range from 500° to 2000°F maintaining the temperature drop across the specimens below 200°F. Average precision of the results was ±7 percent while the accuracy was established to be ±10 percent based on initial calibration. The thermal conductances in air environment were between 60 and 100 percent above comparable values for the panels tested under vacuum conditions. Analysis of the results indicated that gaseous conduction and convection accounted for only a small fraction of the difference, the main effect being a large increase in the radiative contribution produced by increased emittance of the alloy through surface oxidation. Extensive spectral emittance measurements were made and then integrated to provide input data on temperature dependent total emittance to allow quantitative assessment of these radiative contributions.

Analytically predicted thermal conductances were based on a semi-empirical approach suggested by Swann which accounts explicitly for variations in panel geometry, panel temperature drop and materials properties (emittance and metallic thermal conductivity). Agreement with the experimental results was within a few percent at the highest test temperatures for both the vacuum and air environment conditions. At lower temperatures in air environment the agreement was not as good, the predicted values averaging about 15 percent below the experimental data. The overall agreement between predicted and measured conductances measured in vacuum was within about 10 percent which is particularly significant because errors here in the approximated radiation interchange factors would lead to the largest errors in predicted conductance due to high reflectivity and specularity of the honeycomb cells. As a result of this experimental substantiation over a wide variation in dependent parameters it is concluded that the prediction procedure is generally useful for most engineering applications in estimating the thermal conductance of metallic honeycomb composites at high temperatures.

Previous pages were blank, therefore not filmed.

TABLE OF CONTENTS

ILLUSTRATIONS

ILLUSTRATIONS (Continued)

TABLES

SYMBOLS

A = cross-sectional area available for solid conduction, in^2

E_{BB} = blackbody emissive power, $BTU/hr\text{-}ft^2$

F = geometrical view factor

$\mathcal{F}$ = net radiation interchange factor

h = thermal conductance, $BTU/hr\text{-}ft^2\text{-}°F$

k = thermal conductivity, $BTU/in/hr\text{-}ft^2\text{-}°F$

1 = thickness, in.

q = heat flux, $BTU/hr\text{-}ft^2$

R = solidity

S = surface area, $in.^2$

T = temperature, °F

β = ratio of hemispherical to normal emittance

γ = length to diameter ratio

δ = distance between centers of differential radiating elements, in.

ϕ = angle between normal to surface and the line

ϵ = emittance

λ = wavelength, microns

ρ = density, lbs/ft^3

σ = Stefan-Boltzman constant, $BTU/hr\text{-}ft^2\text{-}°F^4$

Subscripts

λ, spectral

T, total

N, normal

H, hemispherical

i,j,n, Isothermal element indices

SECTION I

INTRODUCTION

Structural elements of high strength-high modulus honeycomb core construction have been widely employed in tactical and strategic aircraft and in experimental vehicles of the U. S. Air Force. Intricate honeycomb fabrication problems have been resolved sufficiently in the case of the lower temperature aluminum, stainless steel, and titanium alloys to allow their consideration for use in such systems as the B-58, F-104, F-111, RS-70 and the Supersonic Transport. Extensive investigations of fabrication problems and mechanical and thermal properties of honeycomb composites have been conducted recently. (References 1, 2, and 3.)

For higher temperature applications to approximately 2000°F a wide variety of superalloys have been considered for use in honeycomb panel configurations. Both structural and heat shield designs have been developed and fabrication has been successful (References 4 and 5 and Appendix I). Panels of L-605 cobalt superalloy were used in this investigation because the alloy exhibits good oxidation resistance along with a minimum of fabrication problems. The alloy was used successfully in aft panels for the ASSET vehicle and performed satisfactorily under re-entry heating.

At temperatures beyond 2000°F the use of refractory alloys in honeycomb composite configurations has been very limited due to the extreme difficulties encountered in fabrication. TZM molybdenum alloy was among the first considered, the composite manufacturing methods being based to some extent on the results of the extensive fabrication development efforts carried out under the Air Force's Dynasoar program (Reference 6). The embrittlement and poor fabricability of the TZM resulting from recrystallization have been studied in development of honeycomb sandwich fabrication methods (Reference 7). By using high remelt temperature braze alloys TZM honeycomb panels have been produced (Reference 8). Compatibility of the braze alloy and the oxidation resistant coatings was found to be a problem, however. Similar efforts have been directed toward the development of brazing, diffusion bonding and full panel fabrication procedures for D-36 and Cb-752 columbium alloys (References 4 and 7). Brazing and diffusion bonding of tantalum alloys also have been investigated (Reference 8). The efforts on T-111 and T-222 tantalum alloys are continuing with the objective of producing full scale honeycomb composites.

The use of both metallic and non-metallic honeycombs for reinforcement of organic and ceramic matrices has been studied widely. Non-metallic honeycomb reinforcement of silicone ablators is employed in the GEMINI heat shield while similar honeycomb reinforcement is being considered for the thermal protection systems on pilot vehicles in the Air Force's START program. The use of ceramic filled metallic honeycombs in very high temperature thermal protection system components (References 9 and 11) and in uncooled rocket nozzle extensions, as for example the F-1 Saturn engine (Reference 10) are well known.

In the use of these composites it is important to have fairly accurate estimates of their thermal characteristics along with information on tensile, compressive and shear properties. For structural applications a knowledge of the effective thermal conductance and of temperature gradients which are generated in service is necessary in thermal stress analysis. For heat shield applications the effective thermal conductance must be known as a function of temperature level for both transient and steady state heating conditions in order that heat loads on insulative and structural members may be determined. For filled honeycomb composites where the core structures serve as reinforcement, the thermal transport properties are nearly that of the filler material. However, in the case of light weight, unfilled honeycombs, which are more common in most structural and heat shield applications, the heat transport characteristics are quite complex. This is because convection, conduction (both solid and gas phase)

and radiation heat transfer occur simultaneously. The situation is further complicated by the fact that the relative contribution of these various heat transfer modes changes as the temperature level of the composite varies.

A commonly used design approach to partially circumvent the difficulties in estimating heat transfer characteristic, is simply to observe the thermal response of particular panels when subjected to transient heating conditions simulating those expected in service. Panel distortion, attachment stresses and cold face temperature rise are among the parameters measured in obtaining practical data for design. Although satisfactory in some cases, this approach, of course, lacks generality and extensive testing is required each time panel configurations and/or thermal environments change.

The purpose of this investigation was to study in detail the contributions of various heat transfer modes to the overall thermal conductance of metallic honeycomb composites. Steady state tests were utilized throughout in order to study in a thorough and systematic manner the variations in the relative contributions of conductive and radiative heat transport as a function of temperature level. To facilitate study of solid conduction contributions, flat panels of L-605 cobalt alloy were used having variations in core foil thickness and overall panel thickness. Tests were conducted in both air and vacuum environments to assess the influences of gas conduction and panel oxidation on the radiative heat transfer contribution. Extensive measurements of thermal emittance were performed in conjunction with the radiative transport study. The experimental thermal conductance measurements were made to near the failure limits of the L-605 panels: 2100 to 2200°F. Procedures for the fabrication of refractory alloy honeycomb were not sufficiently developed at the time to allow inclusion of such panels in this test program

The analysis of the thermal conductance data utilized approximate finite difference heat balance techniques to consider radiative and conductive heat transfer simultaneously. Comparisons are made between these analytical predictions and the experimental results allowing for temperature variations in alloy thermal conductivity and temperature induced variations in emittance as a result of oxidation. To further assess validity of the analytical predictions, temperature gradient studies were performed with diffusely reflecting cylinders which simulated the honeycomb core geometry assumed in calculation of the radiative interchange factors.

SECTION II

THERMAL CONDUCTANCE MEASUREMENTS

The apparatus used for the thermal conductance measurements was a high temperature guarded hot plate originally designed for the Air Force by Dynatech Corporation, Cambridge, Massachusetts. A complete description of the construction and calibration of the equipment is given by Sparrell, Coumou and Plunkett in Reference 12. Briefly, the design and operation is as follows: The high temperature heating unit shown in Figure 1, is 12 inches by 12 inches overall. It consists of 9 heater blocks, each 4 inches square by 3/4 inches thick which are fabricated from high purity alumina. Each block has a continuous spiral groove which accommodates 40 mil Platinum-40 percent Rhodium heater wire. After placement of the heater windings the spiral groove in each block is filled with a high purity alumina slip-grog cement. Sintering is accomplished by high temperature air firing.

The central main heater block is surrounded by eight guard heater blocks. During operation test specimens are placed on either side of the heating unit, the power dissipation from the main heater providing a controllable heat flux through each specimen. As in conventional guarded hot plate operation, significant lateral heat losses from the main heater are prevented by adjusting the guard heaters until their average temperature (measured near the main heater) is equal to that of the main heater. To allow automatic balancing of the guard heater units with respect to the main heater, two 15 junction differential thermocouples, one on each side of the heating assembly, were used. The output signal controlled power to the guard heaters. Stepless Control Corporation "Power Props" were used as the basic power control units. These operate on silicon controlled rectifiers (SCR) which are regulated from a d.c. input control signal. Successful operation with SCR units rated at 90 amps has been achieved.

Under balanced, steady state operating conditions it is clear that the power dissipation from the four "corner" guard heater blocks will be greater than that from the four "side" guard heater blocks. In order to make relative power adjustments between these, separate power props with control voltage trimmers were used for the side and corner guard heaters. Once the relative proportion of power was established, the entire guard ring was controlled automatically relative to the main heater.

The overall configuration used during the honeycomb conductance tests is shown in Figure 2. The high temperature heater assembly is sandwiched between two honeycomb panel specimens. Because the panels have relatively thin, electrically conductive face sheets, the various instrumentation thermocouples could not be mounted flush with the specimen surface. After spot welding to the panel face sheet, the 10 mil Platinum/Platinum-10 percent Rhodium thermocouple wires were run into two-bore alumina tubes which were in turn cemented to the panel surface. Couples were mounted on the face sheet in positions directly over core joints and in positions where the face sheet spanned the core cells. This instrumentation procedure necessitated the use of a spacer material between the specimen panels and the main-guard heater unit to accommodate the couples while at the same time providing uniform support for the heater blocks. A 1/8-inch layer of 40-mesh bubble alumina was used for this purpose. Figure 3 shows the honeycomb test panels with the temperature sensing and differential thermocouples in place. The differential couple was, of course, electrically insulated from the specimen surface. The thermocouples over the corner and side guard heater areas were used for control purposes as discussed earlier.

For materials and composites which contain substantial void areas, convection contributions could cause a difference in the effective thermal conductance between the specimen located above the main heater and the specimen located below. Since the power dissipation of the main heater represents the sum of the heat fluxes through the metered area of both specimens,
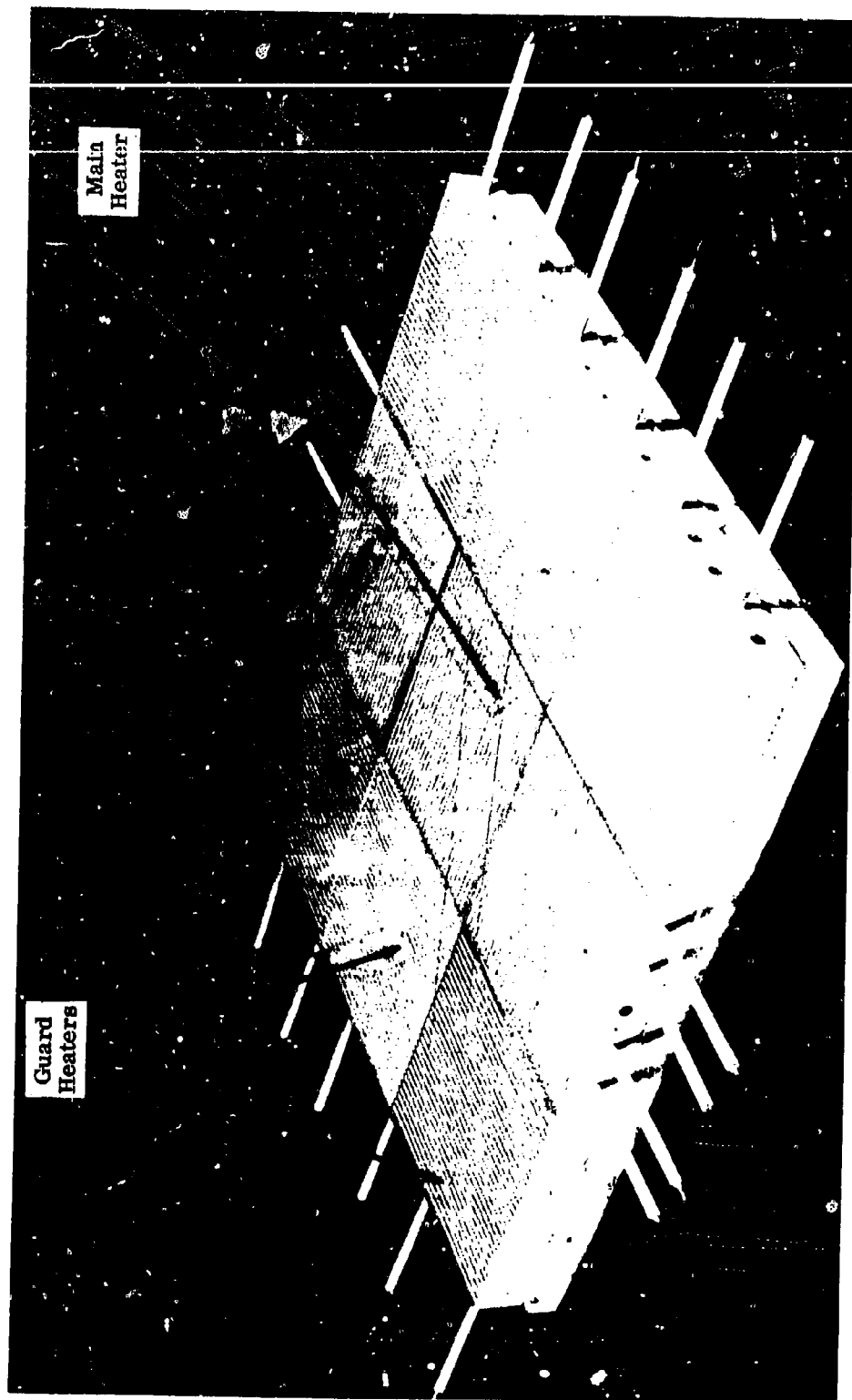
Figure 1. Main and Guard Heater Configuration

HEAT SINK

AUXILIARY HEATER

MULLITE RATIO ELEMENT

UPPER SPECIMEN

| GUARD HEATER | MAIN HEATER | GUARD HEATER |

LOWER SPECIMEN

MULLITE RATIO ELEMENT

AUXILIARY HEATER

HEAT SINK

BASE PLATE
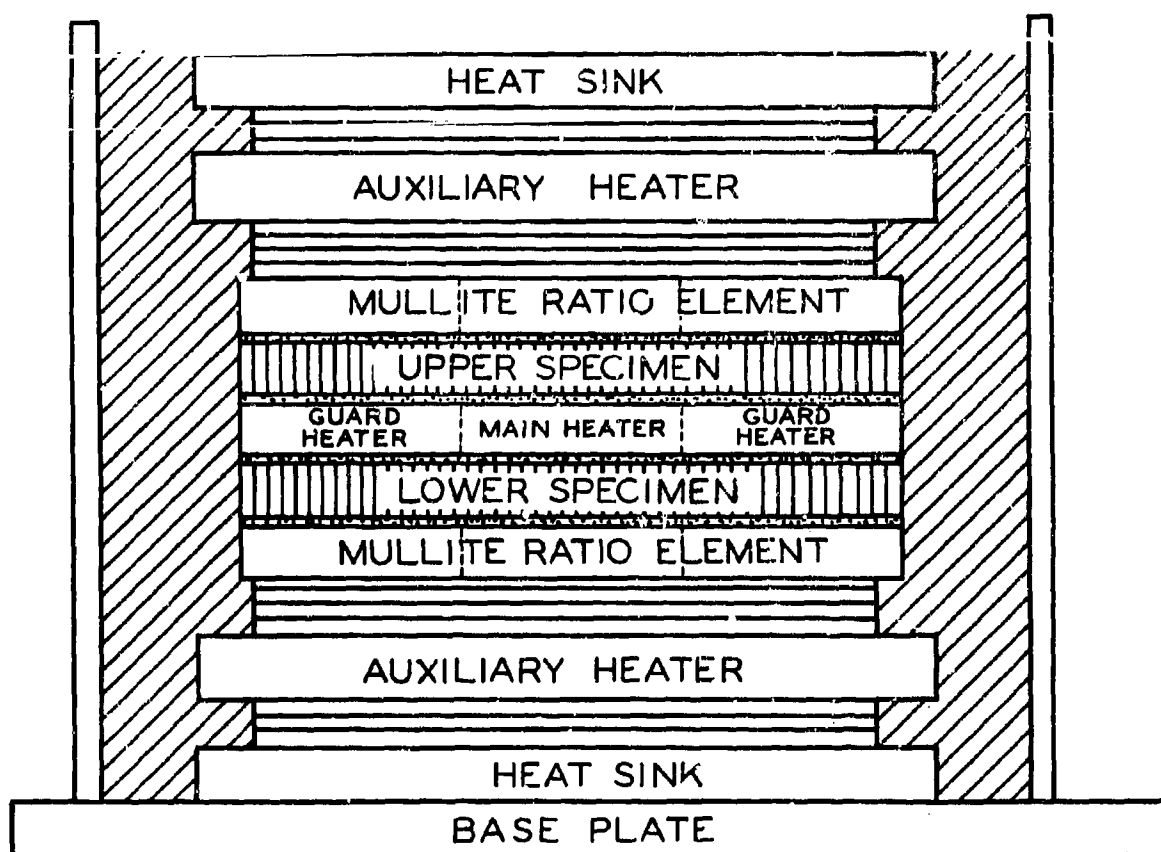
VX REFRACTORY INSULATION

ALUMINA BUBBLE INSULATION

MICROQUARTZ FIBROUS INSULATION

Figure 2.   Test Stack Configuration

5
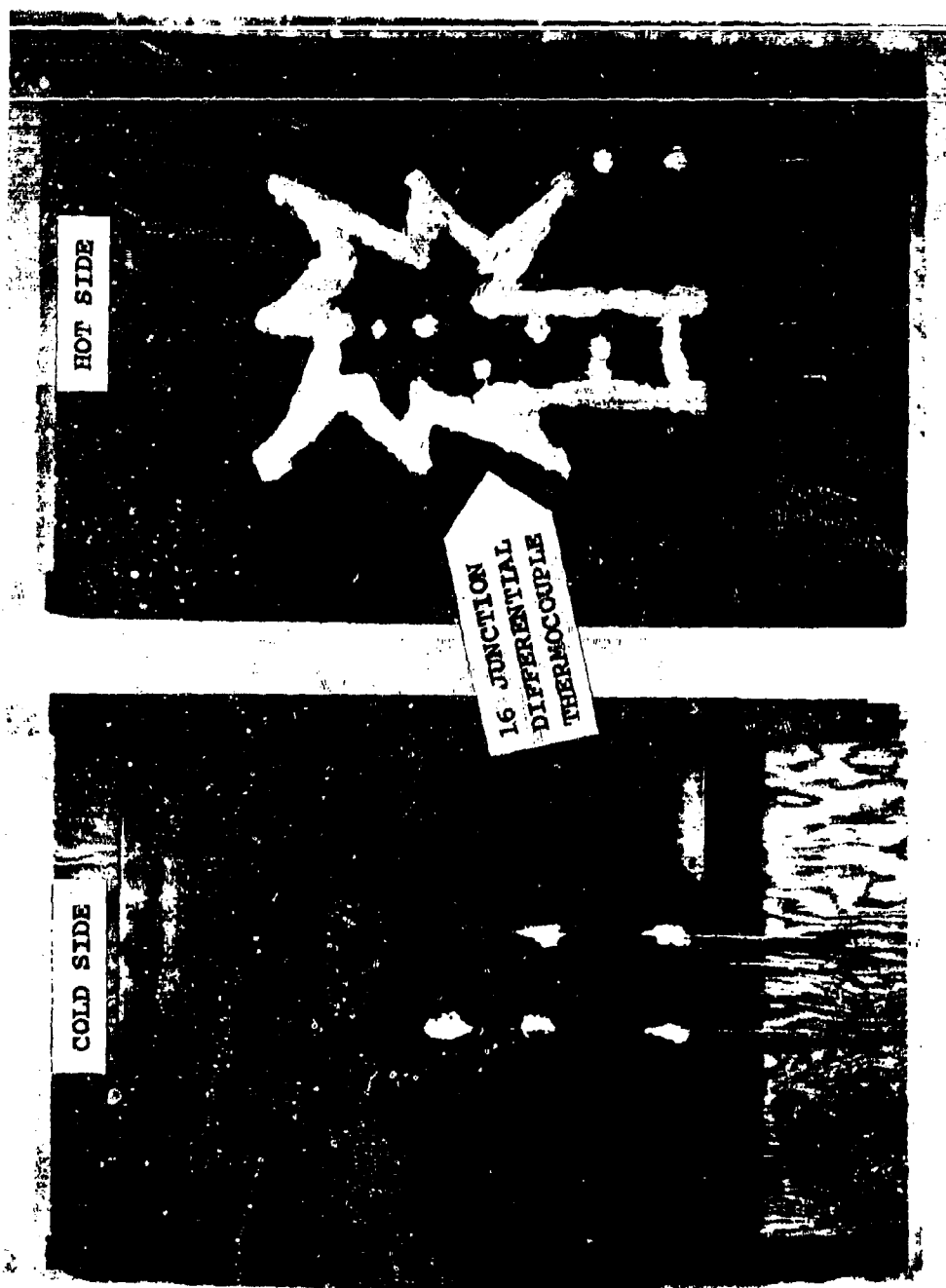
Figure 3. Honeycomb Panel Instrumentation

an independent measurement was required to give the relative proportion of heat going through each specimen. This was accomplished by placing identical heat meters or ratio elements adjacent to the cold face of each specimen as shown in Figure 2. The heat meters were built up from 4-inch square blocks 1-inch thick and were fabricated from commercial aluminum silicate (Mullite). If the mean temperatures of these ratio elements are equal and their thermal conductivity linear over the temperature range considered, the ratio of their respective temperature drops is equal to the ratio of the heat fluxes flowing through them. Measurement of this ratio allows calculation of the heat flux flowing through each specimen. This arrangement also allows simultaneous testing of specimens of different conductivity. Other heat meters of high purity alumina or silicon carbide may be used depending on the temperature range and specimen conductivity range encountered. For all honeycomb panel tests, identical panels were used above and below the main heater. In order to allow independent variation of the specimen cold face temperature during test, auxiliary heaters are interposed between the ratio elements and the water cooled heat sinks. With this arrangement accurate adjustment of the specimen temperature drops could be attained despite the rapid variation in honeycomb specimen conductance with temperature. One auxiliary heater was controlled manually, the other automatically controlled with respect to it. The control signal for this second auxiliary heater was from the thermocouples sensing the temperature drops across the ratio elements; balance between the two auxiliary heaters was achieved when the two ratio elements had the same mean temperature.

Depending on the temperature range of operation the entire assembly shown in Figure 2 was insulated laterally with either Johns-Manville MicroQuartz insulation (to 2000°F) or Norton coarse-grain alumina granules (to 2800°F). An overall view of the equipment during test stack construction is given in Figure 4.
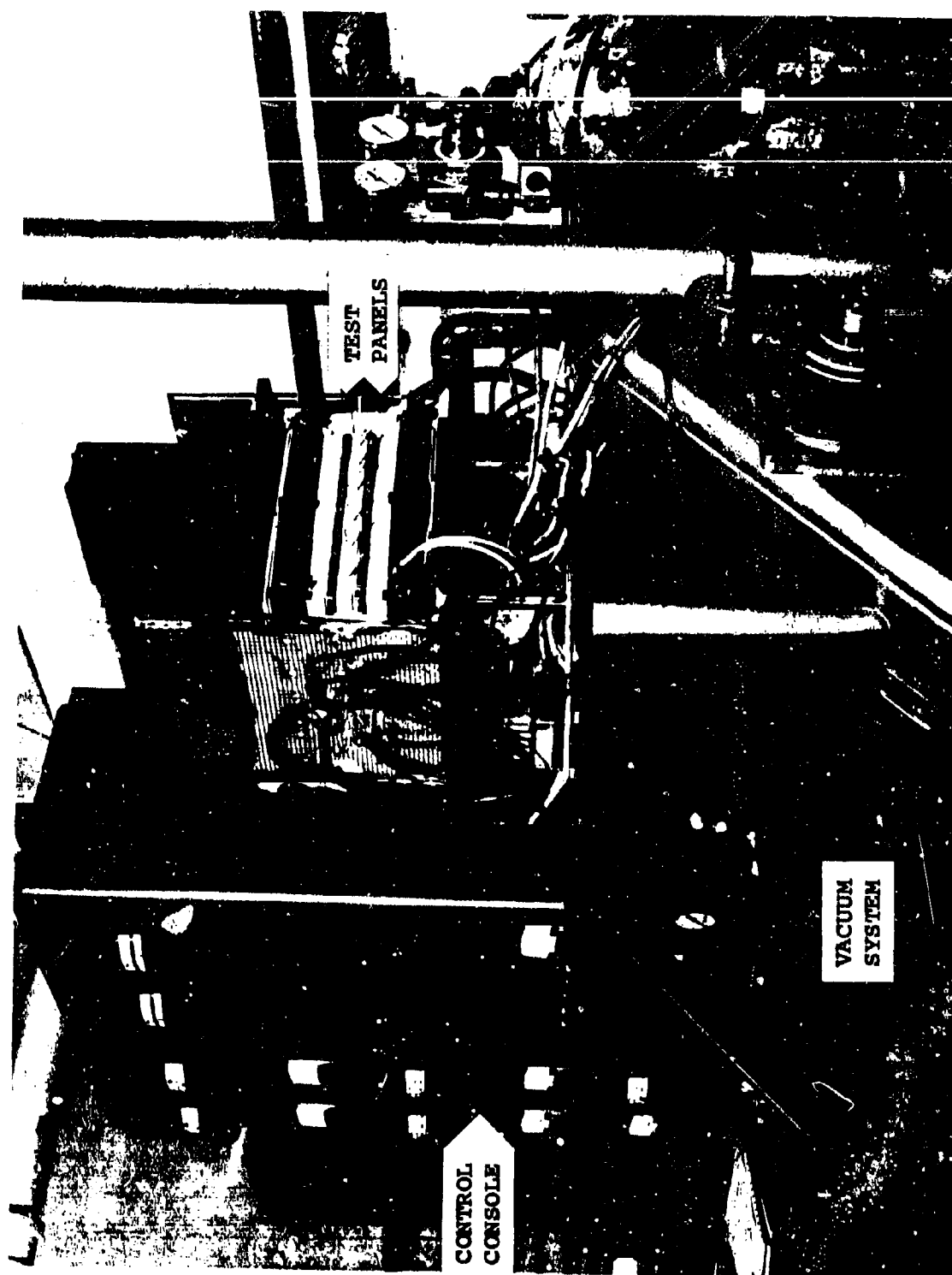
Figure 4. Experimental Test Setup

8

SECTION III

TEST SPECIMENS

The test specimens used in this program were fabricated for the Air Force Materials Laboratory by Solar Division of the International Harvester Company, San Diego, California. The specimens, of L-605 cobalt - base alloy, were in the form of flat panels, 12 inches square. A photograph of a typical panel with edge members in place but before face sheet attachment is shown in Figure 5. Two panel thicknesses and two different foil gages for the core cell were used. The exact geometry of the various test panels is given in Table I. As mentioned earlier, two panels of identical geometry were required for each test in the high temperature guarded hot plate apparatus.

A complete description of panel fabrication process used by Solar along with photomicrographs of core node, node-face sheet and core-face sheet areas are included in Appendix I. Briefly, the procedure was as follows. After hand honing of the core blankets to eliminate rounding of the foil edges and to assure flatness, the edge frame was attached to the core by microtacking, producing the assembly shown in Figure 5. The braze alloy was then applied to the surface of the core in powdered form. After positioning of the face sheets, the panels were individually assembled into a retort unit for brazing. This operation was conducted in two steps. First, to complete the braze the retort assembly carrying the panel was heated in argon to approximately 1950°F, held for a few minutes and then cooled, the cycle requiring slightly over one hour. Second, a diffusion cycle of approximately 3 hours at 2100°F was run to permit homogenization of the braze reaction zone which increases the remelt temperature to about 2300-2400°F. X-ray analysis and ultrasonic scanning were used to produce facsimiles of the panel surfaces. In general, the diffusion bonding was found to be excellent for all panels. The continuity of the braze is shown in Figure 6 which is a photograph of a panel cut at 45°. Note the core perforations which were made to allow panel testing in various gaseous environments. As is shown in the photomicrographs, Appendix I, the minimum fillet-diffused method used in panel fabrication produced panels with very little geometrical distortion due to face sheet and core fillets.

Figure 5.   Honeycomb Panel Before Attachment of Face Sheet

TABLE I

HONEYCOMB TEST PANEL GEOMETRY

Panel Nr.	Panel Thickness, (in)	Cell Wall Thickness, (in)	Face Sheet Thickness, (in)	Core Cell Size, (in)
1A	0.748	0.001	0.010	0.25
1B	0.742	0.001	0.010	0.25
2A	0.380	0.001	0.008	0.25
2B	0.370	0.001	0.008	0.25
3A	0.375	0.002	0.010	0.25
3B	0.375	0.002	0.008	0.25
4A	0.747	0.002	0.010	0.25
4B	0.746	0.002	0.010	0.25

OTHER DATA

Material: 55% Co, 20% Cr, 15% W, 10% Ni (L-605 Alloy)

Braze Alloy: 91.2% Ni, 4.5% Si, 2.9% B, 1.1% Fe (Coast Metals Alloy No. 52, AMS Spec 4778)

Panel Configuration: All specimens were 12 inches square, with perforated core, and 0.025 inch edge members

Figure 6.   45° Section of a Brazed L-605 Honeycomb Panel (2X)

SECTION IV

EXPERIMENTAL RESULTS

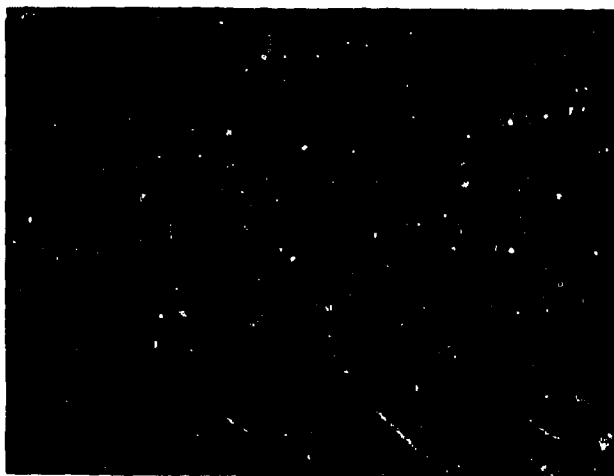The thermal conductance of honeycomb composites is generally defined as the net heat flux through the panel divided by the overall temperature drop as indicated in Equation 1.

$$h = \frac{q}{\Delta T} \qquad (1)$$

where,

$h =$ thermal conductance, $BTU/hr\text{-}ft^2\text{-}°F$

$q =$ specimen heat flux, $BTU/hr\text{-}ft^2$

$\Delta T =$ specimen temperature drop, $°F$

The experimental data obtained during this program was presented in this form. The results obtained during the sequence of four tests, with the four sets of specimens described in Table I, are given in Figures 7 through 9. The tabulated data points are included in Appendix IV. A thermal conductance curve was first obtained under vacuum conditions which ranged from 1×10^{-4} torr to 5×10^{-5} torr, and then under oxidizing conditions in air at atmospheric pressure. During the measurements a period of between 8 and 24 hours was required to reach steady-state conditions before recording each data point. Longer adjustment periods were required at low test temperatures because of comparatively high thermal inertia of the system. Thus approximately 5 days of continuous operation was required for each thermal conductance run. At steady-state the average temperature difference between the corner and side guard heaters was 1-3°F at all temperature levels while the difference between the guard ring and the main heater ranged from 0.3° to 5°F. These measurements were made between the thermocouples mounted on the specimen surfaces directly opposite the various heater blocks. In one air environment test, at about 1500°F, the guard heaters were purposely imbalanced by 40°F with respect to the main heater. The resulting conductance value was compared with a data point at the same temperature taken when the maximum difference between guard and main heaters was 2.3°F. The difference in calculated conductance values was about 7 percent.

To assess the effects of thermocouple contamination from contact with the L-605 several tests were run comparing standard Platinum /10 percent Rh thermocouples with thermocouples which had been spot welded to the L-605 specimens and which had been used in both vacuum and air environment conductance tests. Initial difference of between 3° and 15°F were observed among the various couples; however, these differences remained nearly constant, independent of thermal history and independent of whether the couples were in contact with the L-605 or not. It was concluded that contamination effects were of small importance and that initial thermocouple calibrations were maintained to within a few percent throughout the test sequence on each set of panels. Relative variations among the various couples on a given panel as a function of thermal and environmental history were negligible.

A full analysis of the data will be given in the next section. However, there are several general features which should be noted here. First, the thermal conductance, as defined by Equation 1, is approximately doubled when the panel thickness is halved (comparing Figures 7 and 8, and the two curves in Figure 9). Second, on shifting from a vacuum environment to an oxidizing environment the conductance for a given panel thickness increases greatly (Figures 7 and 8). The air environment curves in these figures lie between 60 and 100 percent above the

Figure 7. Thermal Conductance as a Function of Mean Honeycomb Panel Temperature in Air and Vacuum Environments: Panels 1A and 1B (Panel Thickness: 3/4-inch)
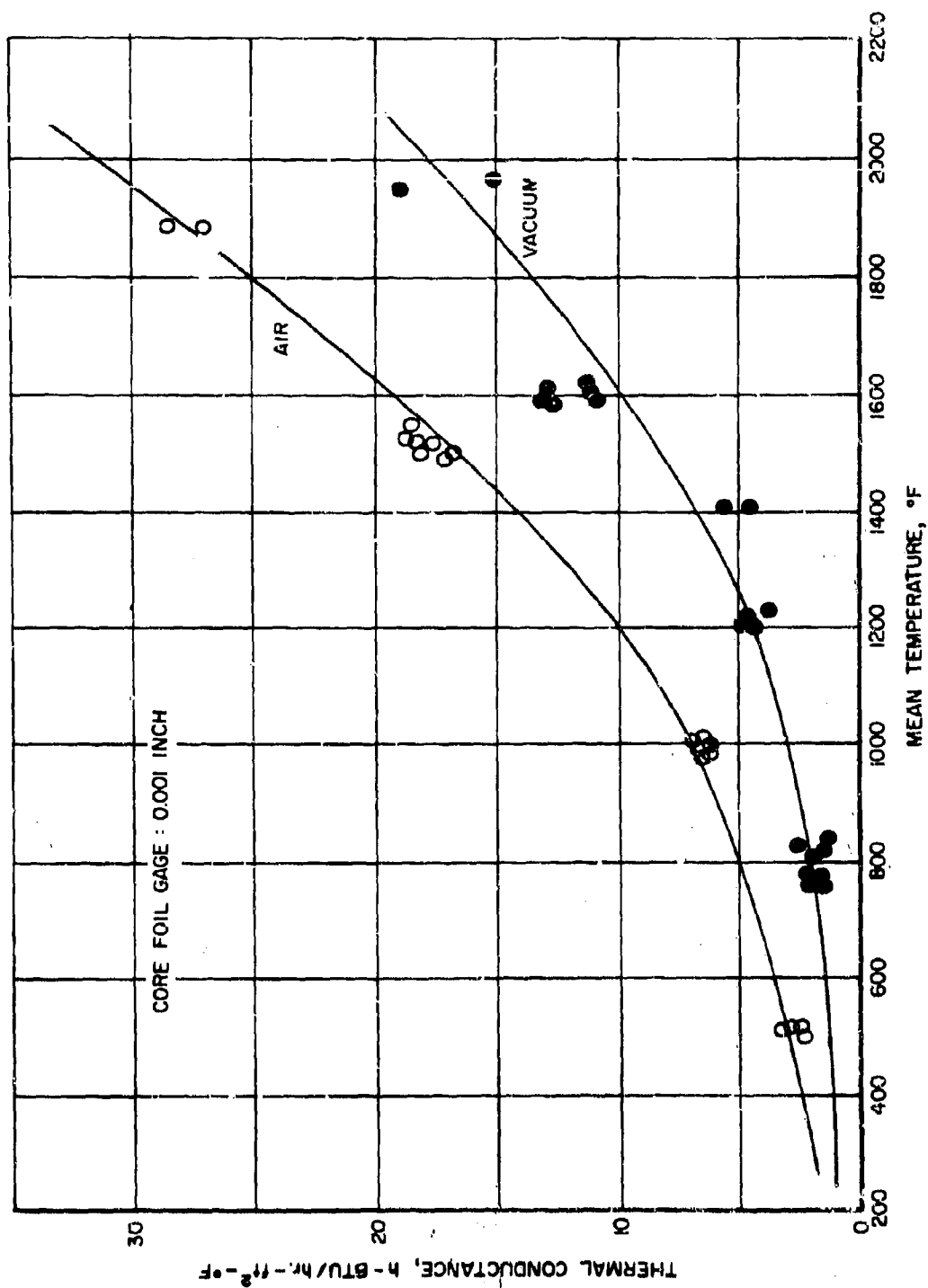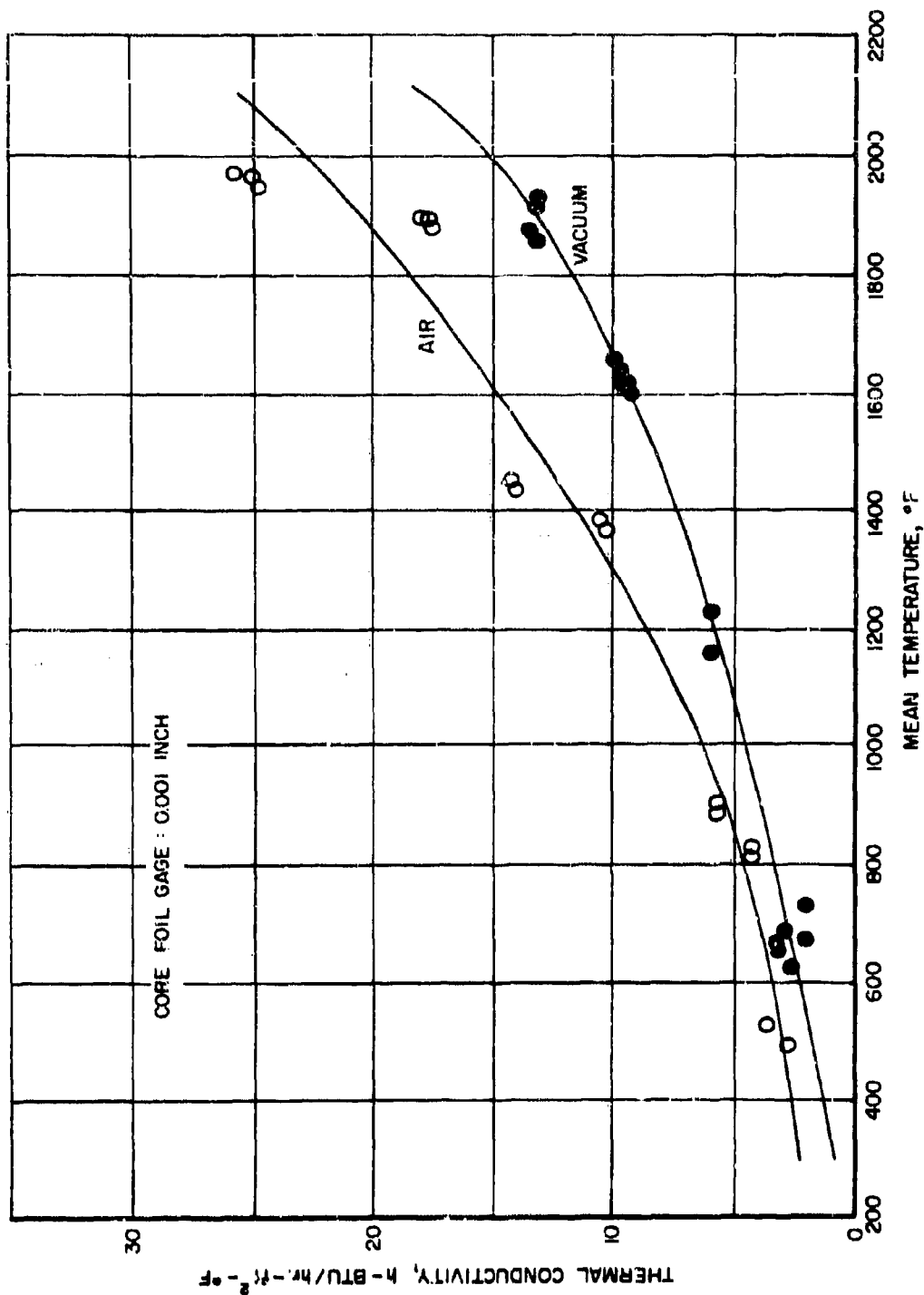
AFML-TR-65-233

Figure 8. Thermal Conductance as a Function of Mean Honeycomb Panel Temperature in Air and Vacuum Environments: Panels 2A and 2B (Panel Thickness: 3/8-inch)
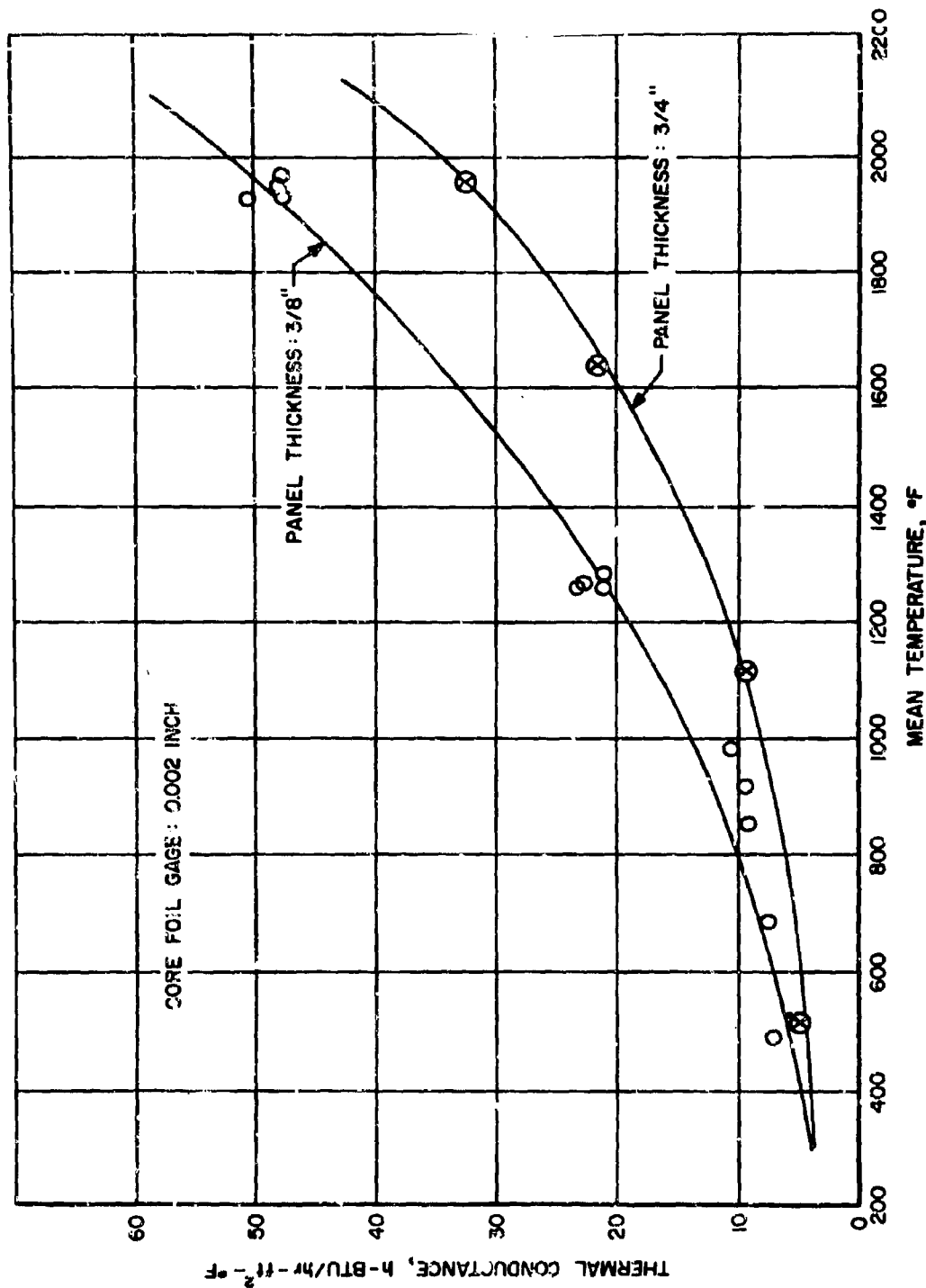
13

Figure 5. Thermal Conductance as a Function of Mean Honeycomb Panel
Temperature in Air Environment: Panels 3A, 3B, 4A, 4B

corresponding vacuum curves. The most obvious factor to consider in accounting for the observed differences is the contribution of gaseous conduction and convection. The gas conduction contribution at 2000°F is approximately 1.4 BTU/hr-ft^2 for the thinner panels and about 0.7 BTU/hr-ft^2 for the thicker panels. Thus this contribution accounts for only about 4 percent of the observed increase at the maximum test temperature. At around 400°F, the gas conduction contribution is about 10 percent. The convection contribution was estimated from the functional dependence of the Nusselt number on the Grashof number-Prandtl number product for the free convection case. The calculated convective contribution is about 3 percent at 2000°F and less than 1 percent at 400°F.

Experimental results in air environment for panel sets No. 1 and No. 3 show the conductance values for the panels above the main heater unit ran about 5 percent higher than the values for the panels situated below the main heater. Although this is about the difference expected from convection effects, the results are not conclusive since the average precision of the data was in this same range, running from ±1.5 percent to ±15 percent. In addition, the trend was not observed in panel set No. 2. It is concluded that the scatter in the experimental thermal conductance data is too high to definitely isolate the 1 to 3 percent difference expected from convective effects.

The large differences between the air and vacuum environment data can obviously not be explained entirely on the basis of gaseous conduction and convection contributions. Because the L-605 alloy oxidizes at higher temperatures it was expected that increased emittance could lead to the increased thermal conductance in air environment if the change was substantial. To investigate this possibility, spectral emittance measurements were made on L-605 in various states of surface oxidation. A full description of these results and the procedure for obtaining the emittance data is given in Appendix II. Briefly the method was as follows: Spectral normal emittance was measured with a Perkin-Elmer Model 13-U double beam recording spectro-photometer using an emittance furnace to hold the specimen and a Gier-Dunkle cavity as the blackbody reference. The system was first calibrated with National Bureau of Standards references, the results being within ±2 percent. The data on the L-605 specimens was then reduced by referring it to data on the NBS oxidized Kanthal reference run simultaneously. The more important observations are summarized in Figure 10 where the spectral normal emittance is plotted for different environmental exposures. The lower curve in Figure 10 is typical of an unoxidized metal in the infrared. After exposure to 2000°F in a 5 x 10^{-5} torr vacuum it is seen that the alloy is slightly oxidized. Exposure at this temperature level in air produces a surface which is heavily oxidized and which has a much higher spectral emittance characteristic of an oxide dielectric as shown in the Figure. At low temperatures the air environment thermal conductance curves begin above the vacuum environment curves due to the slight oxidation encountered under high temperature vacuum conditions. Only the air environment results for panel sets 3 and 4 are shown in Figure 9 since undetermined oxidation occurred during this particular vacuum test. These effects are discussed quantitatively in the next section.

In the heat balance equations the total hemispherical emittance of the L-605 as a function of temperature and environment was required. In order to obtain this information the spectral normal emittance data was converted to total hemispherical emittance. The first step was graphical integration of the spectral normal data according to Equation 2.

$$\epsilon_{TH} = \frac{\beta \int_0^\infty \epsilon_{\lambda N} E_{BB}(\lambda) \, d\lambda}{\int_0^\infty E_{BB}(\lambda) \, d\lambda} \cong \frac{\beta \sum_{\lambda_1}^{\lambda_2} \epsilon_{\lambda N} E_{BB} \, \Delta\lambda}{\sum_{\lambda_1}^{\lambda_2} E_{BB} \, \Delta\lambda} \qquad (2)$$
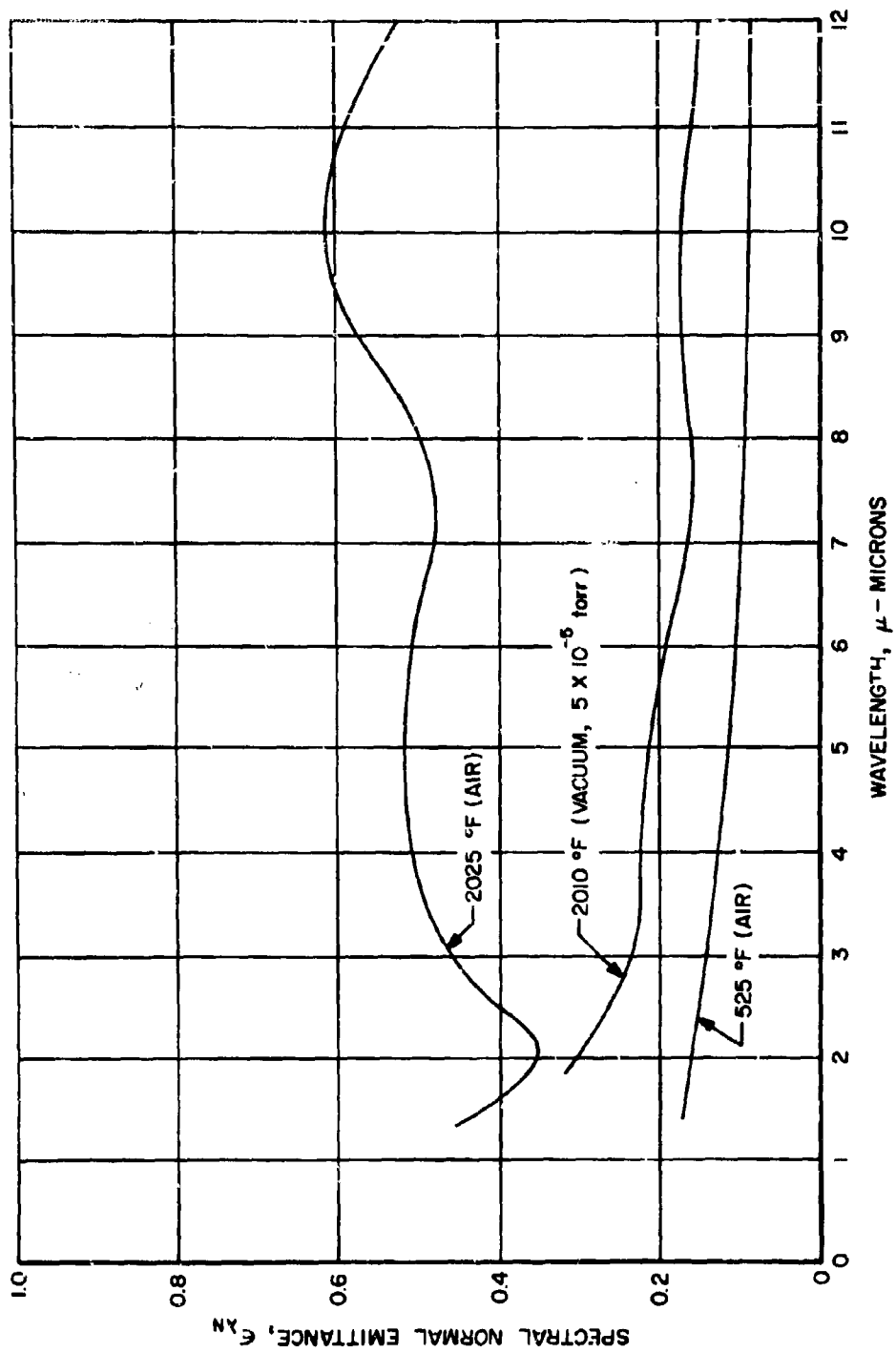
Figure 10. Spectral Normal Emittance of L-605 Cobalt Alloy as a Function
of Temperature in Vacuum and Air Environment

where,

ϵ_{TH} = total hemispherical emittance

$\epsilon_{\lambda N}$ = spectral normal emittance

β = ratio of hemispherical to normal emittance

E_{bb} = blackbody emissive power

λ = wavelength

The resulting total normal emittance data was converted to total hemispherical emittance data using calculated values of the ratio between the total normal and total hemispherical emittance, β . This ratio written explicitly as a function of the optical constants is obtained from the integrated Fresnel equations. The ratio including both perpendicular and parallel polarization components is given as a function of optical constant values by Dunkle (Reference 14). Visual examination of the L-605 specimens was used to ascertain whether the surfaces were essentially metallic or whether oxidation had been extensive enough to develop a surface film characteristic of a dielectric. The optical constants and consequently the value of β will be different for each case. Table II presents the results.

TABLE II

TOTAL HEMISPHERICAL EMITTANCE OF L-605 COBALT ALLOY AS A FUNCTION OF TEMPERATURE AND ENVIRONMENT

Temperature, °F	ϵ_{TH}	$\beta = \epsilon_{TH}/\epsilon_{TN}$ (14)
Vacuum Environment (1 x 10^{-4} torr)		
525	0.123	1.15
1300	0.192	1.13
2025	0.300	1.07
Air Environment (Atmospheric Pressure)		
525	0.123	1.15
1050	0.184	1.12
1230	0.588	1.13
1450	0.582	1.02
1750	0.595	1.13
2025	0.487	1.04

The emittance variation between the vacuum and air environments is by a factor of from 2 to 3 in the temperature range from 1200 to 2000°F. The discussion of results shows that the radiative heat transfer contribution to the total conductance increases from about 60 percent to 80 percent over the same temperature interval. Thus, the observed increase in emittance and the increased contribution in radiative heat transfer at high temperatures is sufficient to account, at least qualitatively, for the large increase observed in thermal conductance in air environment.

SECTION V

DISCUSSION OF RESULTS

Analysis of the heat transfer characteristics of honeycomb composites with open cells is complicated by the fact that both conduction and radiative heat transfer may be important, the relative proportion of each varying markedly with temperature. Because of the strong interdependence of these heat transfer modes at higher temperatures simple superposition cannot be employed in determining the overall thermal conductance of these composites. If radiation contributions are small, which may be the case at lower temperatures, both the steady-state and transient heat transfer properties of a honeycomb composite can be obtained explicitly through transform techniques since linear boundary conditions can be written for the time dependent Laplacian equation. For this case the small radiative contributions can be estimated independently. For example, in early studies of heat transport in honeycombs at Langley, it was found that the radiative contributions could be calculated based on the magnitude of the temperature difference across the panel when only conduction was considered (Reference 15). Thus it was possible to estimate both radiation and conduction contributions based on results for the conduction case only. Experimental verification of this approach was limited to low temperatures.

A more general method for estimating thermal stress distributions and thermal conductance characteristics which would be accurate at higher temperatures requires the use of analog or digital computer techniques in handling the non-linearities. Conversion of the non-linear ordinary differential equations resulting from the one-dimensional conductive-radiative heat balance to finite difference form is one of the most common approaches and is amenable to digital computer solution. In writing the finite difference equations the honeycomb core cell is broken down into a number of rings, which are assumed to be isothermal. A steady-state heat balance written around a given ring would take the following form assuming that only solid conduction and radiation are significant,

$$\frac{T_{n-1} - T_n}{\dfrac{I_{n-1}}{2 A_{n-1} k_{n-1}} + \dfrac{I_n}{2 A_n k_n}} - \frac{T_n - T_{n+1}}{\dfrac{I_n}{2 A_n k_n} + \dfrac{I_{n+1}}{2 A_{n+1} k_{n+1}}} + \sigma \, \epsilon_n \, S_n \left\{ T_n^4 - \sum_{i=1}^{j} \mathcal{F}_{n,i} \, T_i^4 \right\} = 0 \quad (3)$$

Solid Conduction	Solid Conduction	Net Radiation
Into Ring n	Out of Ring n	Transfer From Ring n

where,

T_n = mean temperature of ring n, °F

I_n = vertical thickness of ring n, in.

A_n = cross-sectional area of ring n for solid conduction, in^2

k_n = thermal conductivity of ring n, BTU/hr-ft^2-°F

σ = Stefan-Boltzmann constant, BTU/hr-ft^2-°F^4

ϵ_n = total hemispherical emittance of ring n

S_n = surface area of ring n

$\mathcal{F}_{ni}$ = radiation interchange factor between node i and node n

j = total number of rings in the core cell

19

Aside from the rather involved problem of simultaneous solution of these equations written over the j rings making up the cell core a major difficulty encountered in using Equation 3 is determining the radiation interchange factor $\mathcal{F}_{n,i}$. Using the notation of Hottel (Reference 16) this factor accounts for multiple reflections from all elements that eventually result in a net interchange between ring "n" and ring "i".

If blackbody conditions are assumed (reflectance = 0, and isotropic emission) reflections within the core cell between the various rings do not occur and the net interchange factor reduces simply to a geometrical view factor, $F_{n,i}$. This factor is simply the fraction of the radiant energy emitted by ring "n" which is incident directly upon ring "i". In general, for two arbitrarily placed areas, S_n and S_i, the geometrical view factor is given as follows,

$$F_{n,i} = \frac{1}{\pi S_i} \int_{S_i} \int_{S_n} \left[\frac{\cos \phi_i}{\delta} \right] \left[\frac{\cos \phi_n}{\delta} \right] dS_n \, dS_i \tag{4}$$

where,

ϕ_i = angle between normal to surface i and the line δ

δ = distance between centers of the differential areas dS_i and dS_n

Evaluation of this factor for a variety of geometries such as parallel plates, disks and planes at right angles has been carried out (References 16 and 17). For the case of honeycomb cells Swann (Reference 18) has developed equations for the view factors $F_{n,i}$ in terms of the length to diameter ratios of a cell approximated as a right circular cylinder. The axial symmetry of the geometry allows extensive simplification of the final equations through various reciprocity relationships.

If the emittance of the radiating elements in the honeycomb core is less than unity (reflectance > 0) a much more complex radiation interchange within the core will occur. If the reflectance is low the direct view factor, $F_{n,i}$, can be used without appreciable error. If the reflectance is high (low emittance) the net interchange factor $\mathcal{F}_{n,i}$ which accounts for multiple reflections should be employed. It is clear that while $F_{n,i}$ is exclusively a function of geometry, $\mathcal{F}_{n,i}$ is a function of both geometry and the optical properties of the core material. As will be shown $\mathcal{F}_{n,i} = f(F_{n,i}, \epsilon)$ if simplifying assumptions are made concerning the emittance ϵ. First, it is assumed that all surfaces obey Lambert's Cosine Law, that is, they are diffuse emitters and reflectors. Second, it is assumed that gray body conditions are met. Figure 10 shows that neither metallic nor oxidized L-605 are gray body emitters; however, since an emittance correction is made in the heat-balance equations at each temperature level and since the overall temperature drop across the panels is low at all temperature levels, gray body emission is a valid approximation.

Considering the finite difference area elements or "ring's" of a honeycomb core cell shown in Figure 11, the direct radiation from element (1) to element (2) is $\epsilon F_{1,2}$; of this the fraction $(1-\epsilon)F_{2,3}$ is reflected from element (2) to element (3) and finally the fraction $(1-\epsilon)F_{3,1}$ of this beam is reflected back to element (1). Thus for this particular beam a series of the form given in Equation 5 is developed to account for multiple reflections. Expanding similar equations to include multiple reflections from all elements has been carried by various investigators including the effects of absorbing gases (References 16, 18, 19, 20, and 21).
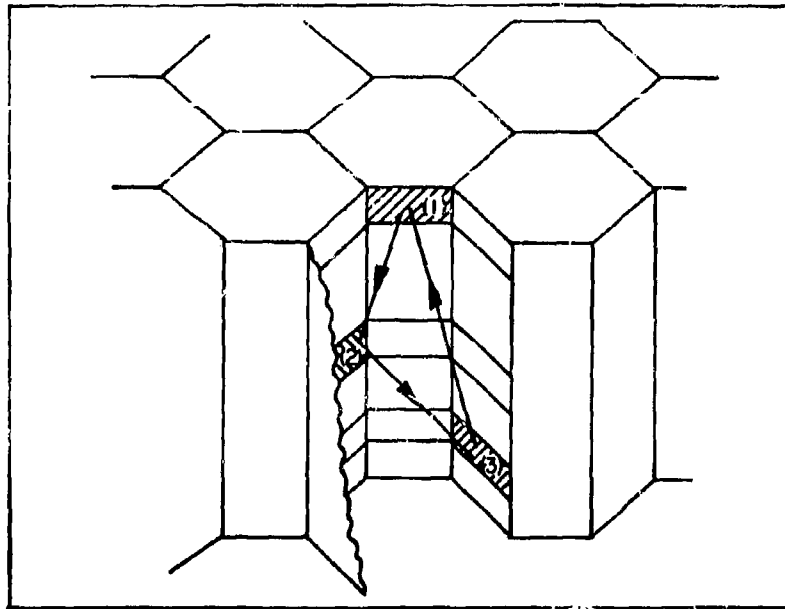
Figure 11. Finite Difference Elements Within Honeycomb Core Cell

$$\mathcal{F}_{\substack{\text{one beam,}\\ \text{2 reflec.}}} = \epsilon F_{1,2} + (1-\epsilon)\,\epsilon\, F_{1,2}\, F_{2,3} + (1-\epsilon)(1-\epsilon)\,\epsilon\, F_{1,2}\, F_{2,3}\, F_{1,3}$$

$$= \epsilon \left[F_{1,2} + (1-\epsilon) F_{1,2} F_{2,3} - (1-\epsilon)(1-\epsilon) F_{1,2} F_{2,3} F_{3,1} \right] \tag{5}$$

The following closed form expression for $\mathcal{F}_{n,i}$ encompassing "j" finite difference areas was developed by Swann (Reference 18):

$$\mathcal{F}_{n_0, n_i} = \epsilon_{n_i} \left[F_{n_0,n_i} + \sum_{n_j=1}^{j} (1-\epsilon_{n_0}) F_{n_0,n_i} F_{n_0,n_i} + \sum_{n_j=1}^{j} \sum_{n_k=1}^{j} (1-\epsilon_{n_j})(1-\epsilon_{n_k}) F_{n_0,n_i} F_{n_j,n_k} F_{n_k,n_0} + \cdots \right] \tag{6}$$

where,

$$n_0,\, n_1,\, n_j,\, n_k = \text{various rings of the cell}$$

Alternately if the j by j matrices $\left[F \right]$ and $\left[\mathcal{F} \right]$ and the diagonal emittance and reflectance matrices $\left[\epsilon \right] = \text{diag}(\epsilon_1,\, \cdots \epsilon_j)$ and $\left[\rho \right] = \text{diag}\,(1-\epsilon_1 \cdots 1-\epsilon_j)$ are defined,

$$\left[\mathcal{F} \right] = \sum_{i=0}^{\infty} \left[[F][\rho] \right]^i [F][\epsilon] \tag{7}$$

Using the factor $\mathcal{F}_{n_i}$ or an approximation to it in Equation 3, it is possible to write a set of similar equations over all the finite area elements of the honeycomb cell including the hot and cold face sheet elements (Reference 22). From these equations the temperature distribution down through the cell can be determined. Once this is known, an overall heat balance gives the steady-state heat flux through the entire core due to simultaneous solid conduction and radiation, q_T. Based on this quantity an effective thermal conductance, h_e, is defined as

$$h_e = \frac{k_e}{l} = \frac{q_T}{\Delta T_T} \tag{8}$$

where,

k_e = effective thermal conductivity of the honeycomb panel,
BTU-in/hr-ft^2-°F

l = overall panel thickness, in.

T_T = overall panel temperature drop, °F

Since computations of effective conductances based on Equations 3 and 7 are highly involved and require extensive computer analysis, it was desired to compare the experimental results obtained in this investigation with analytical predictions based on approximated radiation interchange factors and heat balances which could be applied conveniently in engineering practice. The semi-empirical method suggested by Swann (Reference 18) was the most satisfactory. It was found that the effective thermal conductance of an open-celled honeycomb composite could be written as a function of the cubic power of the honeycomb face sheet temperatures when the net radiation interchange factor was written in the following form,

$$\mathscr{F}(F, \epsilon) = 0.664(\gamma + 0.3)^{-2.62} \epsilon^{(1.63)(\gamma + 1)^{-0.89}} \tag{9}$$

where,

γ = honeycomb cell length to diameter ratio

The comparisons are given in Figures 12 through 14 where the curves drawn through the experimental data points in Figures 7 through 9 are replotted along with dotted curves representing the analytical predictions. The gas conduction contribution has been added to the analytical curves for the air environment case. These analytical values were first expressed as dimensionless effective thermal conductivity, $\overline{k}_e$, versus dimensionless temperature, $\overline{T}_i$, and then converted to dimensional form for direct comparison with the experimental results. $\overline{k}_e$ and $\overline{T}_i$ are defined as follows,

$$\overline{k}_e = \frac{k_e}{k R} \tag{10}$$

$$\overline{T}_i = \left[\frac{\sigma l R}{k} \right]^{1/5} T_i \tag{11}$$

where,

k_e = effective thermal conductivity, BTU-in/hr-ft^2-°F

k = thermal conductivity of the core material,
BTU-in/hr-ft^2-°F

R = ρ core/ρ = solidity

ρ_{core} = core density, lbs/ft^3

ρ = density of metal making up the core, lbs/ft^3

l = core height, in.

σ = Stefan-Boltzmann Constant, BTU/hr-ft^2-°F^4

22

Figure 12. Thermal Conductivity of 3/4-inch Thick (0.001 inch core)
Honeycomb Panels as a Function of Temperature: Comparison
of Experimental Results With Analytical Predictions
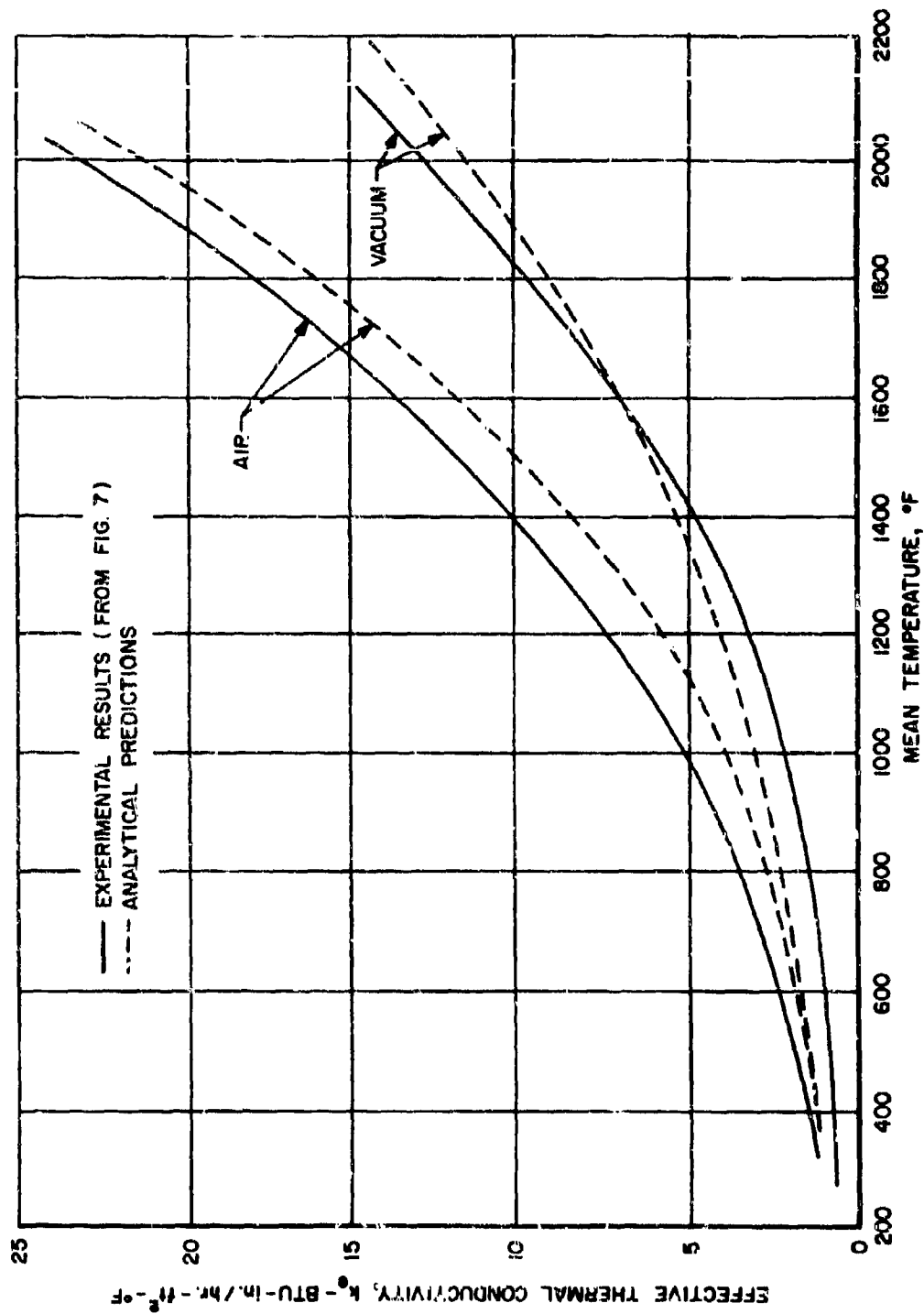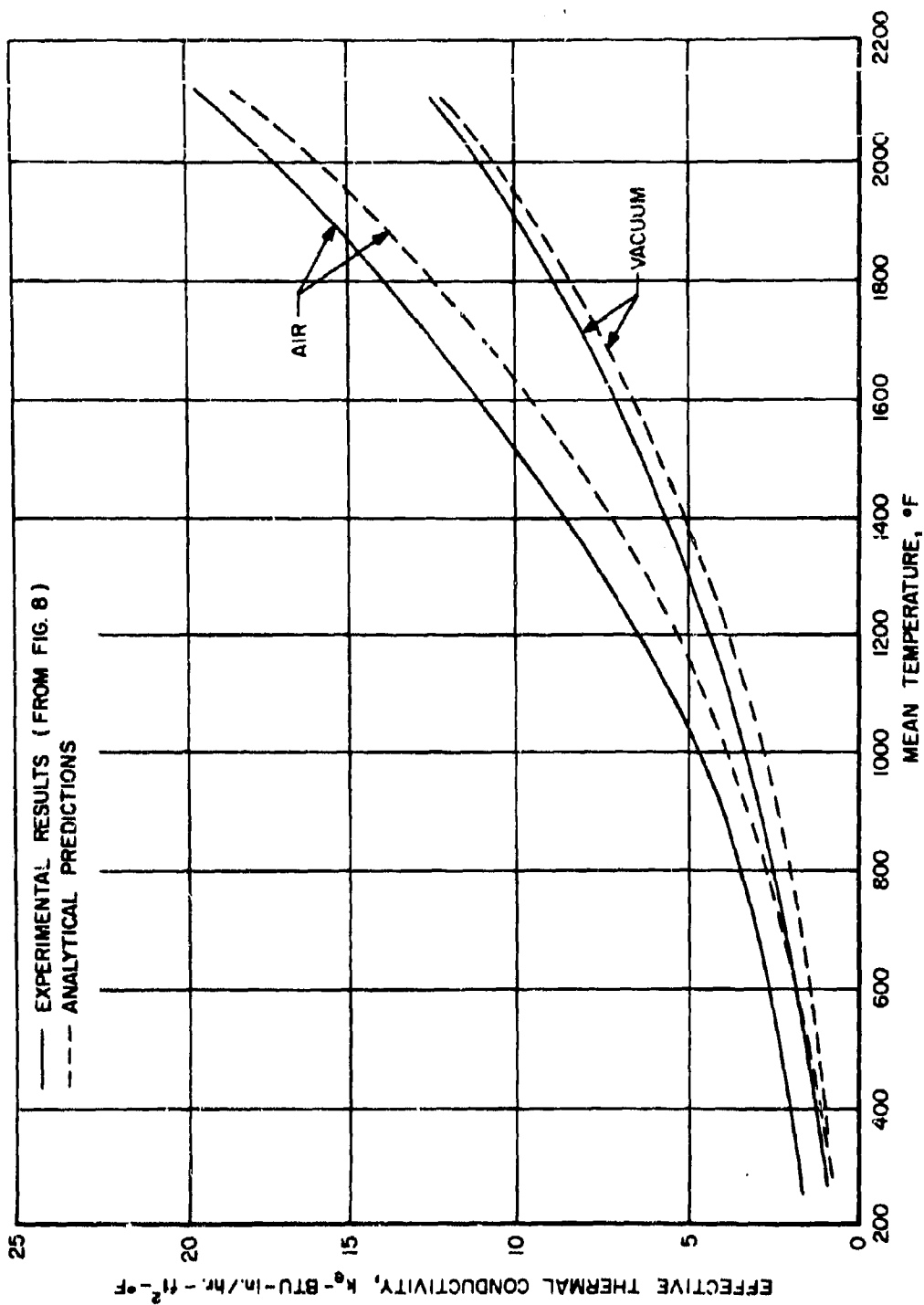
Figure 13. Thermal Conductivity of 3/8-inch Thick (0.001 inch core)
Honeycomb Panels as a Function of Temperature: Comparison
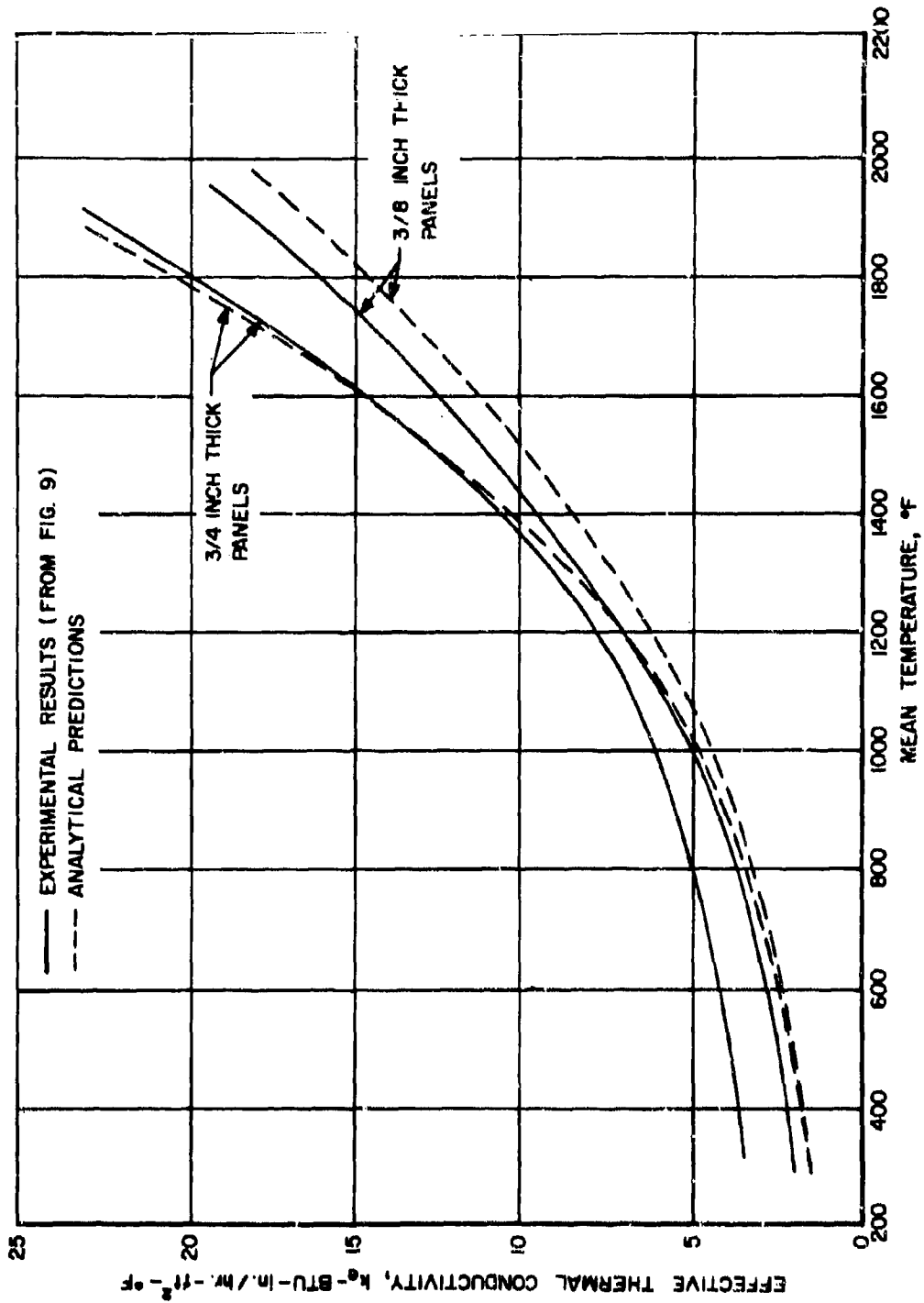of Experimental Results With Analytical Predictions

Figure 14. Thermal Conductivity of 3/8 and 3/4-inch Thick (0.002 inch core) Honeycomb Panels as a Function of Temperature in Air Environment: Comparison of Experimental Results With Analytical Predictions

The solidity term, R, is clearly the cross-sectional area of the honeycomb which is available for direct solid phase thermal conduction. In order to allow for conduction contributions from braze alloy flow down the core nodes, this term was calculated from direct weight measurements of the fabricated core. This procedure was more accurate than estimates made from photomicrograph cross-sections. It is also evident that the product k x R represents the fraction of heat transferred by solid conduction and thus $\bar{k}_e$ as given in Equation 10 is essentially the ratio of the total heat transfer due to solid conduction and radiation to the heat transfer by solid conduction alone. Values of $\bar{k}_e < 1$ indicate solid conduction predominance; values of $\bar{k}_e > 1$ indicate radiation predominance. The relative solid conduction and radiative contributions for these panels as a function of temperature and test environment will be discussed after examination of the comparisons in Figures 12 through 14.

Agreement between the predicted conductivity and the experimentally measured values is generally very good. On the average, the analytically predicted curves are about 30 percent below the experimental curves at low temperatures with the average difference decreasing to only 6 percent at the maximum test temperature. In all cases the analytical values were derived making allowances for temperature dependent thermal conductivity of the L-605 and for variations in total emittance as a function of test environment and temperature level as experimentally measured and reported in Table II. The close agreement between measured and predicted values for the vacuum environment tests is particularly noteworthy since errors in the approximated radiation interchange factors would be expected to cause the largest errors in effective panel conductivity when the emittance is low or where core reflectance and specularity is high. The vacuum environment emittance data in Table II shows that the reflectance was indeed quite high ranging from 0.70 to 0.88.

At lower temperatures the predicted values, as shown in Figures 12 and 13, are nearly identical in air and vacuum since the emittance values are about the same. The curves in Figures 12 and 13 were obtained with honeycomb panels having a core with 0.001 inch cell walls which represent a solidity factor of R = 0.85 percent. The panels used in the tests reported in Figure 14 had 0.002 inch core cell walls which correspond to a solidity factor of R = 1.63 percent. The conductivity correlation, which accounts for this variation, is excellent in this case also. At low temperatures where the solid conduction predominates, the solidity governs the conductivity level. At 400°F the average measured thermal conductivity for the panel with 0.001 inch core is 1.6 while that for the panels with 0.002 inch core is 3.4. A similar ratio exists between the analytically predicted values.

In the general definitions of thermal conductivity the parameter is independent of the thickness of the test specimen and of the temperature gradient across it. This is not the case for unfilled honeycomb composites at high temperature for two reasons. First, the net radiation interchange factor is a function of the length to diameter ratio of the cell. Second, even for constant geometry, the radiative contribution varies in a non-linear fashion with temperature level and specimen temperature drop. Thus, the experimental conductivity curve for the 3/8 inch panel in Figure 14 lies below that for the 3/4 inch panel due to the greater temperature gradient in the thinner panels. The overall temperature gradient is accounted for explicitly in the correlation resulting in the spread in the analytical curves. It is important to observe that radiative heat transfer in the cells, together with its strong influence on conductive contributions, particularly at higher temperatures, leads to effective thermal conductivity values which are dependent on both specimen thickness and temperature gradient. This dependence must be considered in practical application of honeycomb composite conductance data.

Returning to discussion of the dimensionless conductivity defined by Equation 10, the solid conduction and radiation contributions summarized in Table III were calculated from the $\bar{k}_e$ values predicted for the various panels.

TABLE III

RADIATION AND SOLID CONDUCTION CONTRIBUTIONS TO THE OVERALL CONDUCTANCE AS A FUNCTION OF HONEYCOMB GEOMETRY, TEMPERATURE LEVEL AND TEST ENVIRONMENT

Solidity = 0.85%				
MEAN TEMPERATURE, °F	PANEL THICKNESS, In	ENVIRONMENT	SOLID CONSTRUCTION CONTRIBUTION, %	RADIATION CONDUCTION, %
780	0.75	Vacuum	42	58
1210	0.75	Vacuum	30	70
1980	0.75	Vacuum	17	83
510	0.75	Air	57	41
1000	0.75	Air	35	63
1880	0.75	Air	10	87
700	0.375	Vacuum	59	41
1250	0.375	Vacuum	35	65
1970	0.375	Vacuum	18	82
900	0.375	Air	41	57
1460	0.375	Air	19	78
1980	0.375	Air	13	84
Solidity = 1.63%				
510	0.75	Air	77	18
1130	0.75	Air	38	58
1960	0.75	Air	13	83
490	0.375	Air	85	10
1290	0.375	Air	34	61
1960	0.375	Air	20	75

Examination of Table III shows that for a fixed panel geometry (constant panel thickness and solidity) the radiative contribution is lower in vacuum environment than it is in air because the emittance is lower. The difference tends to increase with temperature since the emittance of the L-605 increases in air due to oxidation. For a fixed solidity, the solid conduction contribution is higher in the thinner panels for both vacuum and air environments because the thermal gradients are substantially higher. These differences diminish at higher temperatures in both vacuum and air because the relative contribution of radiation increases more rapidly with temperature in the thin panels. This is due to more favorable radiation interchange factors in the shallower cores.

The predominance of radiative transfer at higher temperatures as indicated in Table III is further substantiated through the temperature dependence of the total thermal conductivity curves given in Figures 12 through 14. If an effective conductivity, k_o, is defined where the conduction and radiation contributions are equal, then a plot of the function

$$k(T) = k_0 \left[\frac{T}{T_0} \right]^3 \qquad (12)$$

falls within about 5 percent of the various thermal conductivity curves. If radiation heat transfer predominates a cubic temperature dependence as expressed in Equation 12 is expected in this case where the overall panel temperature drop is small relative to the absolute temperature level.

The differences between the analytical predictions and the experimental measurements at low temperatures are attributed partly to conductance measurement errors and partly to analytical productions which are too low. At higher temperatures where the guarded hot plate accuracy increases, the differences are attributed to small uncertainties in emittance. The fact that the differences between predicted and measured conductance values decrease more rapidly with temperature in the case of the vacuum runs than the air environment runs, substantiate this observation. For shallow core cells such as these encountered here, uncertainties and variations in emittance when the emittance level is moderately high ($\epsilon = 0.5$) have a relatively large effect on the approximate radiative interchange factor. With a core length to diameter ratio of between 1.0 and 3.0 a ten percent variation in emittance leads to a 6-9 percent variation in the thermal conductance at high temperatures. The conductance variation with emittance is less sensitive for the deeper core. Experimentally the agreement was somewhat better at high temperatures for the thicker panels having the deeper core.

Comparisons with results obtained by other investigations are limited because very little experimental data is available in the literature on the thermal conductance of superalloy honeycombs; however, some determinations were made on flat L-605 cobalt alloy panels with 0.002 inch core cell walls (Reference 4). The specimens were fabricated in a manner similar to those used in this investigation. The experimental results were compared with the thermal conductivity data obtained under this investigation on the panels with 0.002 inch foil, Figure 14. The panels tested by North American Aviation as reported in Reference 4, were 0.5 inches thick, the panel temperature drops being comparable to those used here. The comparison showed that the North American data fell midway between the data in Figure 14 for the 0.375 inch and 0.750 inch thick panels. Taking the thickness dependence into account the agreement was within 2 percent over the temperature range covered by North American: 500 to 1600°F. Within experimental precision then, the agreement is exact.

Some additional data on the thermal conductance of L-605 honeycombs were obtained by Dynatech Corporation (Reference 12). The panels used were flat, 0.92 inches thick with 0.0015 inch cell walls. Although no details of the panel fabrication procedure were given it is possible that node flow of braze alloy could have been substantial, increasing the solidity factor greatly. Comparison with the data obtained in this investigation, making allowances for the difference in panel and cell wall thickness, indicated that the Dynatech data was high by about 20 percent at all temperatures from 600 to 2000°F.

Finally, to provide a qualitative check of the predicted non-linear temperature gradients down the walls of a honeycomb cell when both conductive and radiative heat transfer are significant, thermal gradient studies were run on cylindrical elements approximating the cell configuration. Right circular cylinders with length to diameter ratios of 1.0 and 10.0 were fabricated from seamless stainless steel. The steel selected had a thermal conductivity nearly equal to that of the L-605. The cylinders were instrumented axially with thermocouples and were coated on the inside surface with cobalt oxide to give a diffuse finish and an emittance of very nearly 1.0. One end of cylinders were cooled, the other heated to obtain the plots of wall temperature as a function of position given in Figure 15. Further details of the experimental arrangement are given in Appendix III.

In these cavities with large axial temperature gradients direct radiation interchange ($\mathcal{F}_{n,i} = F_{n,i}$; $\epsilon = 1.0$) between portions of the internal surface leads to temperature gradients which may deviate substantially from the nearly linear gradients predicted if only solid conduction were considered. As shown in Figure 15, the gradient near the hotter end of the cell is steeper than the linear gradient case, while the gradient near the center and toward the cooler end is flatter. This occurs because of the direct radiation interchange from the hot end to cooler portions down the wall. When the length to diameter ratio is low (l/d = 1.0) the effective radiation interchange factor is high compared to the factors for the deep cavities (l/d = 10.0). The more pronounced curvature of the dotted curves for the deep cavities in Figure 15 reflects this difference.
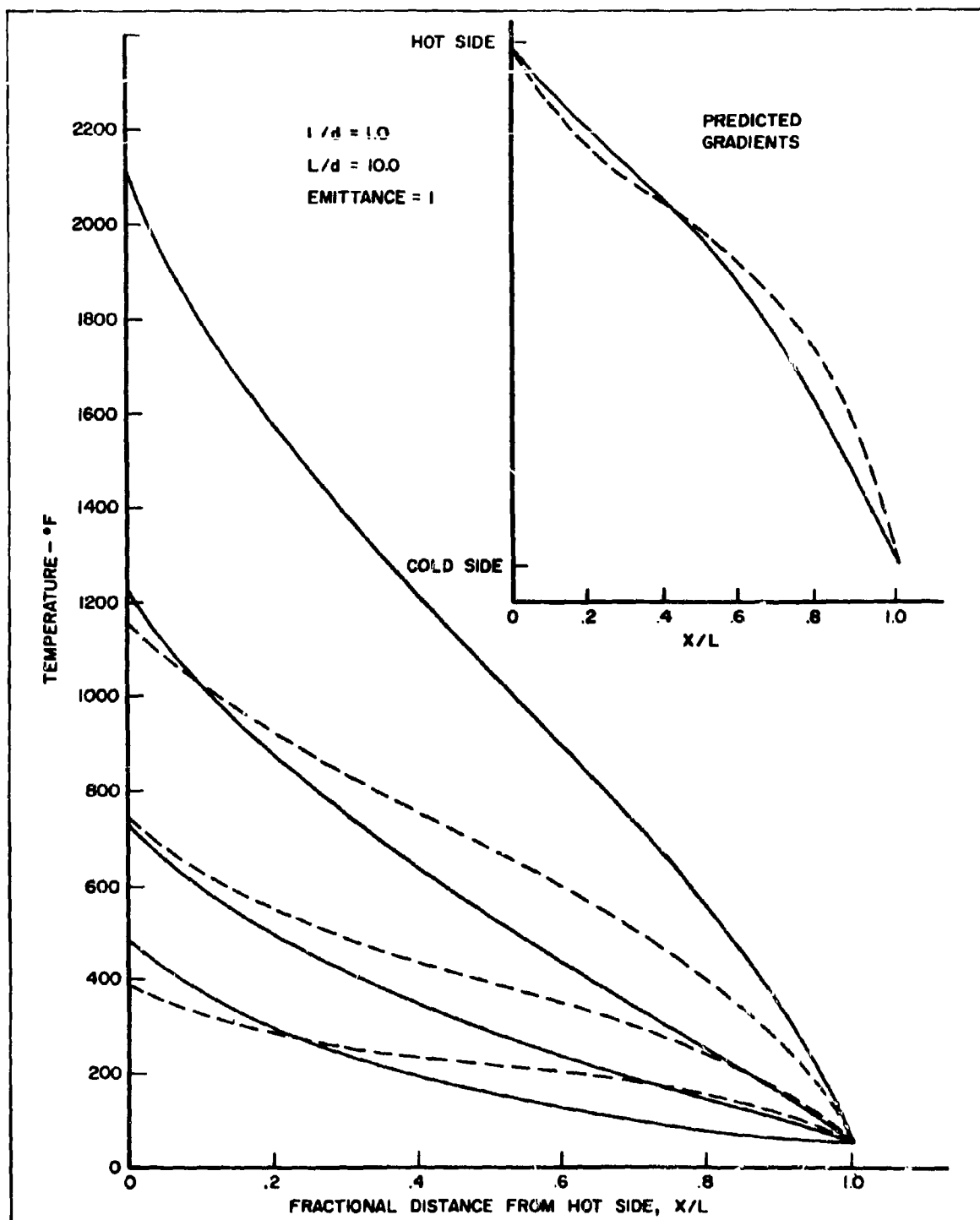
Figure 15.   Temperature Gradient Down a Cylindrical Wall With Solid
Conduction and Internal Radiation ($\epsilon = 1$)

30

SECTION VI

CONCLUSIONS

In general the following conclusions can be drawn regarding the thermal conductance results on the L-605 honeycomb composites.

1. The experimental results which exhibit an average precision of ±7 percent indicate that the thermal conductance of the L-605 honeycomb panels increases with temperature in both vacuum and air environments. This general increase is attributed mainly to increased radiative heat transfer at higher temperatures. The results are in very good agreement with other data reported in the literature.

2. The fact that the air environment conductances for a given panel were 60 to 100 percent higher than the vacuum environment conductances at the same temperature level is due mainly to oxidation of the cobalt alloy resulting in an emittance increase of a factor of 2 to 3 and a proportionate increase in the radiative contribution. Gas phase conduction and convection accounted at most for about 8 percent of the difference.

3. Analytical predictions of honeycomb composite conductances using approximated radiation interchange factors were found to agree with the experimental results to within 6 percent at the highest test temperatures. At lower temperatures the agreement was not as good, the predicted values averaging about 15 percent below the experimental data. The agreement is particularly significant in the case of the vacuum environment curves since errors in approximated radiation interchange factors would have the greatest detrimental influence on the predicted conductance in this case where the core cells are highly reflective, specular surfaces.

4. The radiative contribution to the total thermal conductance was found to increase from about 20 percent at 400°F to about 80 percent at 2000°F. This effect is reflected in the fact that the thermal conductance was nearly cubic in temperature at the higher test temperatures. When high temperature applications are considered the importance of having accurate emittance data on shallow cell honeycomb composites such as those tested here, is clear.

5. Temperature distributions across open celled honeycomb composites in the direction of heat flow are highly non-linear under conditions where radiative contributions are significant. This factor should be accounted for in thermal stress calculations when panel temperature drops are substantial.

6. Because radiative contributions introduce significant non-linearities in the net transport process in open celled honeycomb composites, certain precautions must be exercised in engineering uses of thermal conductance data. The most important point is that the effective conductance values are a function of the temperature drop across the panel as well as the absolute temperature level. In addition, when changes in the emittance of the honeycomb core or the internal surfaces of the face sheets occur substantial variations in effective conductance are likely.

7. The analytical results are sufficiently accurate particularly at the higher temperature which are of most direct interest to allow use of this prediction procedure in engineering design for high temperature applications. The procedure has been demonstrated to be of very general applicability since variations in honeycomb cell geometry, panel thickness, and panel temperature drop are accounted for explicitly. The increased prediction accuracy afforded by more refined analyses involving exact solution of the finite difference heat balance equations is not felt to warrant their use because of the large volume of computer computation required.

SECTION VII

APPENDICES

APPENDIX I

HONEYCOMB PANEL FABRICATION

1. INTRODUCTION

The following description of the panel fabrication procedure used by Solar Division of International Harvester Company is a summary of the final report submitted by the Company under panel fabrication contract, AF 33(657)-11745. The final report was written by Mr. James R. Woodward, Research Engineer, Solar.

2. PANEL FABRICATION

a. Core-Edge Frame Preparation

The brazing process for L-605 honeycomb panels with high temperature capability requires precision contact between the honeycomb core and facing. The mating interface of the core to the facing must be sharp, square-cut and free of burrs. The necessity for the requirement is to permit an exceedingly small and uniform amount of braze alloy to be preplaced at core-facing junction. During the subsequent brazing operation the braze alloy merely melts "in place" at the core-facing joint. Metallurgical reaction of the braze alloy and core-facing interface occurs to precisely controlled depths during a thermal diffusion process. A significant increase in the braze alloy and metallurgical inter-solution of the core and facing occurs to provide high temperature capability.

The diffusion cycle permits homogenization of the braze reaction zone allowing resultant increases in remelt temperatures in the neighborhood of 2300 to 2400°F with the superalloy L-605.

The core blankets as machine made had misaligned ribbons causing faying surface steps of as much as 0.0035 inches. To prepare the edges of the 0.001 and 0.002 inch core ribbon, a freeze fixture was made to secure the core blankets flat. The surfaces were then hand honed with a silicon carbide block. The resulting surface as inspected under 40 power was flat with no rounding of the foil edges.

The core honing operation was accomplished in two stages. The core surface was first honed so that all ribbon steps were removed. The edge frame was then assembled to the core by microtacking and a final honing operation was then performed on the frame to bring it down to the precise level of the core.

The edge frame was made from 0.025 inch L-605 sheet. It consisted of a strip which was formed into a 12 inch square and butt welded. Three 0.187 inch holes were placed in each side of the frame for venting.

b. Braze Alloy Loading

Braze loading of high temperature honeycomb structures is one of the most critical operations. Diffusion controlled brazements require that minimum braze alloy quantities and optimum loading sites be strictly controlled. Before braze alloy loading, the core was cleaned by vapor degreasing, alkaline wash and water rinse. The core was then surface coated with a polybutene film and dipped into the powdered braze alloy. Typical braze alloy pickup is shown in Figure 16. The loading rates averaged 7.83 grams per ft^3 for the 0.002 inch core and 5.40 grams per ft^3 for the 0.001 inch core.
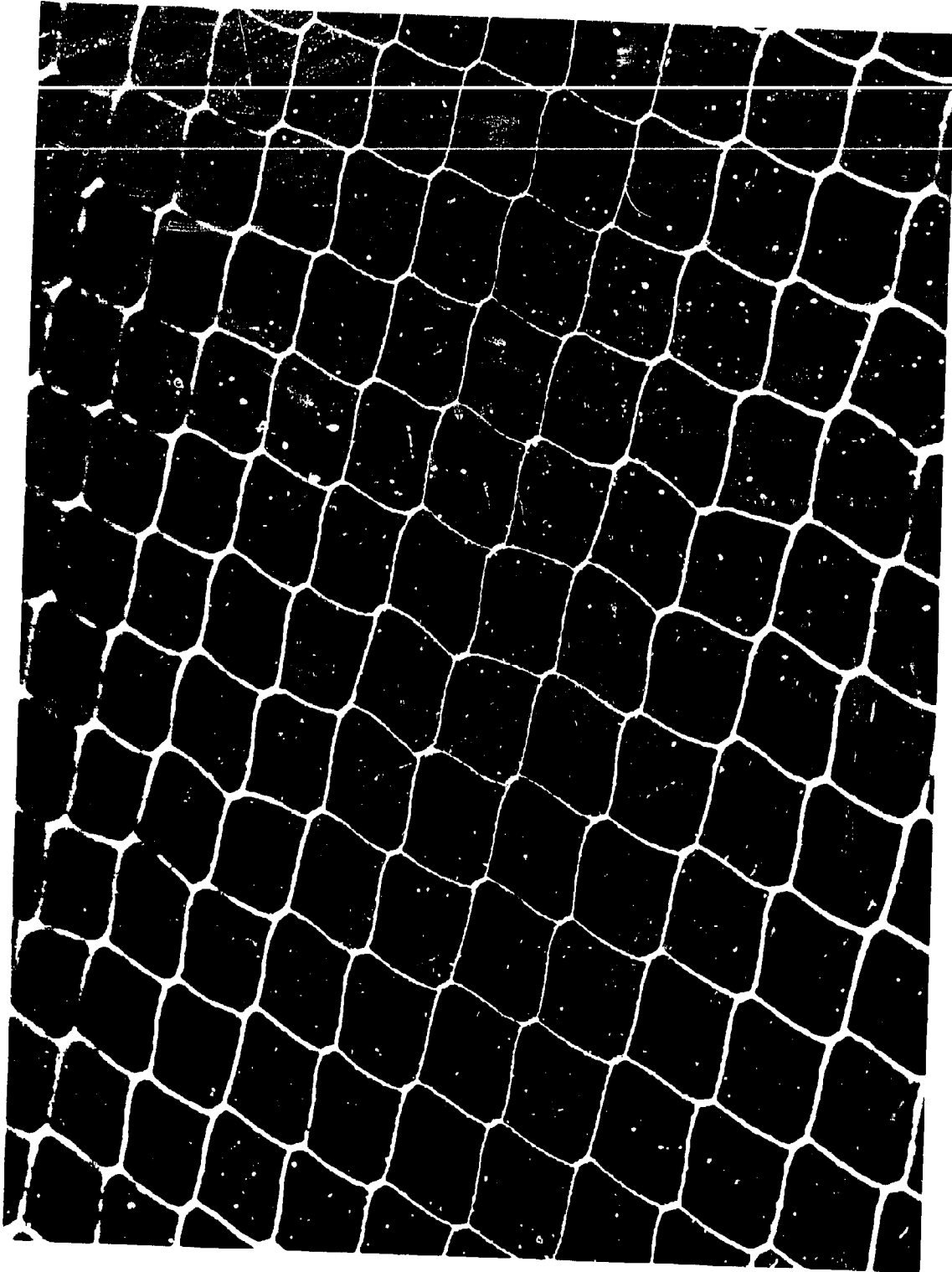
Figure 16. Typical Braze Alloy Loading

c. Panel Layup

The taping sheets were formed into a pan by edge folding 1.2 inch. This procedure allowed better handling conditions and also enabled a cleaner transition to adjacent slip sheets and edge supporting members. Figure 17 shows the face sheet-core layup components. Slip sheets were positioned against the skins to stabilize the retort system. These slip sheets were made from 0.025 Inconel 600 and served to separate the thin skin from the heavier retort bag. Assembly operations such as microtacking the thermocouples to the retort were isolated from the skin by the slip sheets. A 1/2 inch band of Nicro Stop-Off (Wall Colmonoy Co.) was applied to the edge of the sheet and dried by playing a soft flame over the band. A thin coating of colloidal Boron Nitride was then applied over both surfaces of the slip sheet to aid in separating after the brazing and diffusion processes.

Edge filler core was made from 0.010 Inconel ribbon and surface ground to 0.010 inches less than the full panel height. These strips were 1/2 inch wide and were used as transition pieces from the relatively rigid retort edge to the flat pressure applying portion of the retort diaphragm.

The panel-slip sheet-filler core assembly was positioned by microtacked foil taks to afford handling strength. Figure 18 shows the components of this assembly.

The retorts were made from 0.025 inch Inconel formed into a pan as shown in Figure 18. Tubes were welded into two opposite ends for purge and vacuum control. The assembly was accomplished by positioning the panel layup in one retort pan and lowering the other pan in place. The pans were then registered to a flat granite plate by banding a hold down plate to the assembly. While in the registered position the edge of the retort was clamped by mechanical toggle type clamps.

The Assembly in the clamped position was removed from the precision flat and the retort pans edge welded. Welding was accomplished by standard TIG (tungsten inert gas) air cooled hand torch and generator power source using argon as the inert gas. The welded retort assembly was again registered to the precision flat and full vacuum was applied. At this point vacuum was sustained on the system until the brazing and diffusion operations were complete. The vacuum tightness was checked by a one hour hold and observing any drop in the vacuum pressure. At the early stages the leak tightness was checked by Mass Spectrometer-helium leak techniques but the system was found to be reliable without this operation.

d. Atmosphere Control and Thermocouple Assembly

During the vacuum registering phase, the retort was connected to the atmosphere control panel. The argon atmosphere is purified by a titanium getter which is operated at 1350°F, a molecular sieve and cold trap operated at -120°F. The atmosphere is monitored by flow meters and a hot strip checker. The hot strip checker invented by Solar consists of a 4 inch diameter glass vessel which is in series with the outlet line from the work piece so that it always contains a sample of the last gas removed from the retort. A strip of A-286 foil is arranged inside the vessel so that it can be heated by electrical resistance while surrounded by the atmosphere sample. The appearance of the strip after heating in the atmosphere is an effective index of atmosphere quality as A-286 is very sensitive to contaminates.

The pressure is regulated through the panel by valves to achieve any fraction of full vacuum by mixing purified argon on the inlet side of the part. Flows are regulated by valves to allow the required dynamic purge. The pressure and flow are monitored by gages, manometer and flow meters. Actual flows during dynamic purges are on the order of 1 cfh.
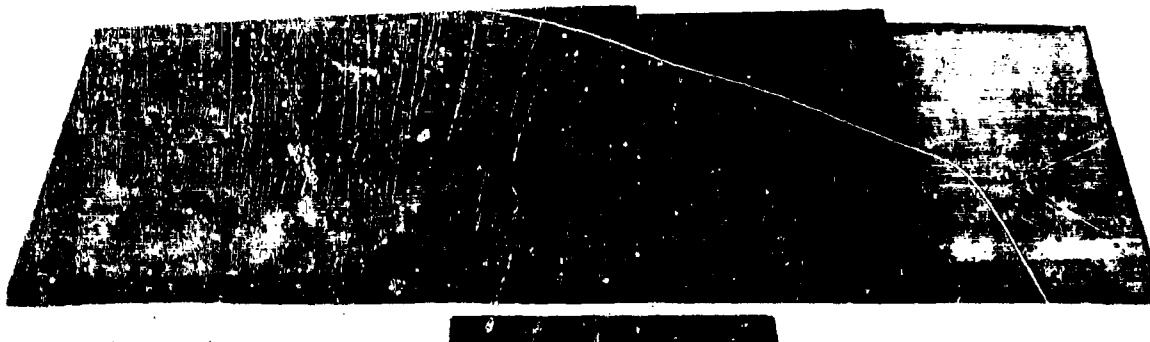
Figure 17. Honeycomb Panel Assembly: Core, Frame, Edge Member

Figure 18. Honeycomb Panel Braze Layup: Core Assembly, Face Sheets,
Slip Sheets, Retort Pan

AFML-TR-65-233

Temperature monitoring was accomplished with six thermocouples located at the top, bottom and center of each side of the panel. They were microwelded to the retort using foil tabs for positioning. The temperature of each thermocouple was monitored by a 12 point recorder. Burner control was adjusted to maintain uniform temperature over the one square foot panel.

e. Panel Brazing

The radiant gas brazing facility described in Reference 23 was used for this program. The device is essentially symmetrical about a vertical plane passing through the entrance slot. On one side of this plane there is a radiant panel composed of seven horizontal rows of burners. Each row contained 16 individual burners fitted against each other. The burners are connected to seven manifolds which are in turn attached to a movable vertical rack permitting precise adjustment of the distance from the radiant panel to the work piece. The panels were set 20 inches apart for the L-605 panels (10 inches from the work piece).

The initial development on the high temperature diffused honeycomb brazing established the braze loading rates, pressure-temperature relationships and process parameters. The pressure-temperature relationship is an extremely important variable which calls for accurate brazing controls. The main parameter is to establish the maximum pressure applied to the facing-core joint without cell buckling.

The limits established for the pressure-temperature programming during brazing of the two different core foil gages is indicated in Table IV.

TABLE IV

PRESSURE-TEMPERATURE RELATIONSHIP
FOR L-605 HONEYCOMB BRAZING

Temperature, °F	Pressure, psia	
	0.001" core	0.002" core
200°F	13.4	13.7
1800°F	1.0	2.6
(Variation is linear between these temperatures)		

A typical braze cycle involved heating to about 1900°F over a period of 30 minutes, holding at this level for about 5 minutes and then cooling at about the same rate. The largest temperature gradient across the retort assembly occurred in the low temperature range of from room temperature start to 1000°F. A 100°F gradient is the approximate maximum which occurs at a 500°F mean temperature. Cool down gradients are fairly well controlled having a 50°F maximum at the start of the cooling cycle.

f. Panel Diffusing

As described earlier, diffusion (or homogenization) of the braze alloy is required to develop high remelt temperatures. In order to accomplish this the panels were exposed to a step type thermal treatment. The furnace for this operation was a natural gas fired, box type furnace which is used for long time, high temperature heat treatments. After part stabilization at 1800°F, the temperature was raised in 50°F steps to 2100°F where it was held for approximately two hours.

38

3. ACCEPTANCE DATA

a. Metallurgical Evaluation

Metallurgical analyses and quality inspections were performed on the L-605 panels. Two specimens were sectioned to evaluate node flow and face sheet-core joints. Figure 19 shows a typical core-face sheet joint with a 7 gram per ft^2 braze loading. A relatively large fillet is obtained at this loading rate. A section through the node area is shown in Figure 20. In this case, diffusion has occurred through the 0.002 inch foil without reduction in gage by solution.

A cross-section of the nodal joint halfway up the 3/4 inch core is shown in Figure 21. Figure 22 is a micrograph of the core-face sheet joint very close to the node point. It shows the start of the node fillet between the core legs.

In measurements of panel flatness it was found that the 3/8 inch thick panels varied up to 0.087 inches from perfect flatness. The temperature gradients developed during the braze operation were sufficient to cause some distortion of the thinner panels. The higher section modulus of the thicker panels prevented significant distortion.

b. Non-Destructive Testing

Minimum fillet, diffused honeycomb panels are relatively unique in the non-destructive testing requirement. The normal honeycomb panels, made by standard processes, have heavy fillets and usually have a braze filler radically different in physical properties (that is, silver or gold). This system lends itself to non-destructive testing by radiography, which is considered a reliable inspection method. The minimum fillet-diffused method of high temperature honeycomb fabrication, however, does not have the same characteristics and therefore is unique. Solar Advanced Research investigated three methods of inspecting the braze bond.

(1) Radiographic Method

The 3/4 inch panels were radiographed and it was noted that there was no definition of core-face sheet joint or node flow. The density and size variations between the braze and L-605 alloys were not sufficient to be detectable by X-ray analysis, in these diffusion bonded panels.

(2) Thermal Sensitive Coating Method

A method which utilized the difference in thermal conductivity between a bonded core and a single face was investigated. This process is based on the fact that the bonded core foil conducts heat away from the skin faster than an unbonded area at the center of the core cell. The material used for this study was Bond Check made by Magnaflux. The process showed very poor sensitivity. It was concluded that the minimum fillet joint does not conduct sufficiently different than the cell center to produce a discernible pattern.

(3) Ultrasonic Method

Ultrasonic techniques for non-destructive testing of honeycomb have advanced to a high degree within recent years. Recent experience on other unique inspection requirements has shown this method to be extremely versatile and reliable. Nine panels were inspected ultrasonically.

The equipment used for this inspection was located at Automation Industries in Torrance, California. A Lithium Sulfate focused transducer was operated at 15 megacycles per second

Figure 20. Core Node – Face Sheet Joint: 0.002 Inch Core – 0.01 Inch Face Sheet (75X) Oxalic Electroetch

Figure 19. Core–Face Sheet Joint: 0.002 Inch Core –0.01 Inch Face Sheet (250X) Oxalic Electroetch

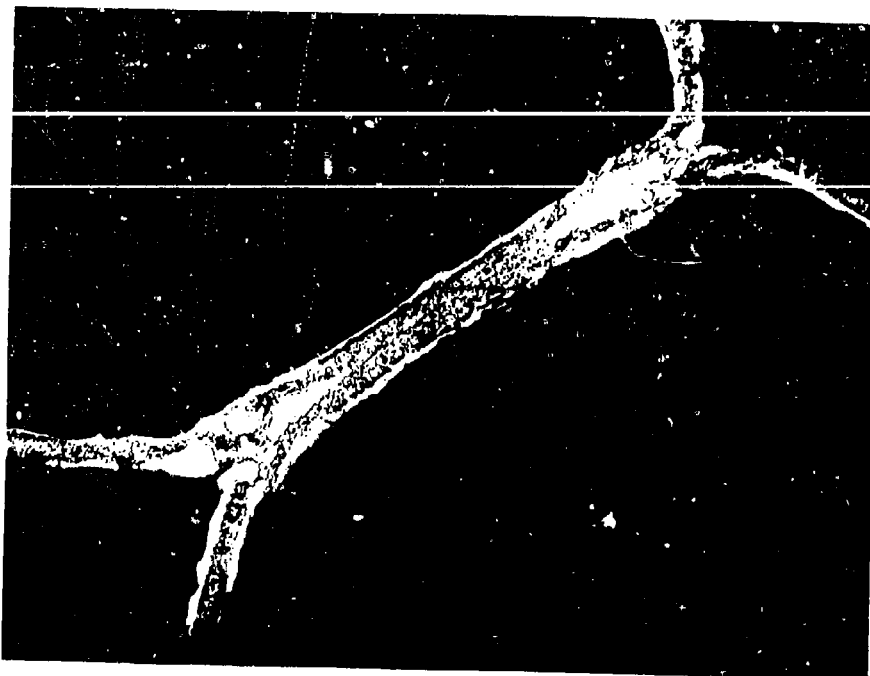Figure 21. Core Node Joint: Section Taken 3/8 inch From Face of a 3/4 inch Specimen (50X) - Oxalic Electroetch
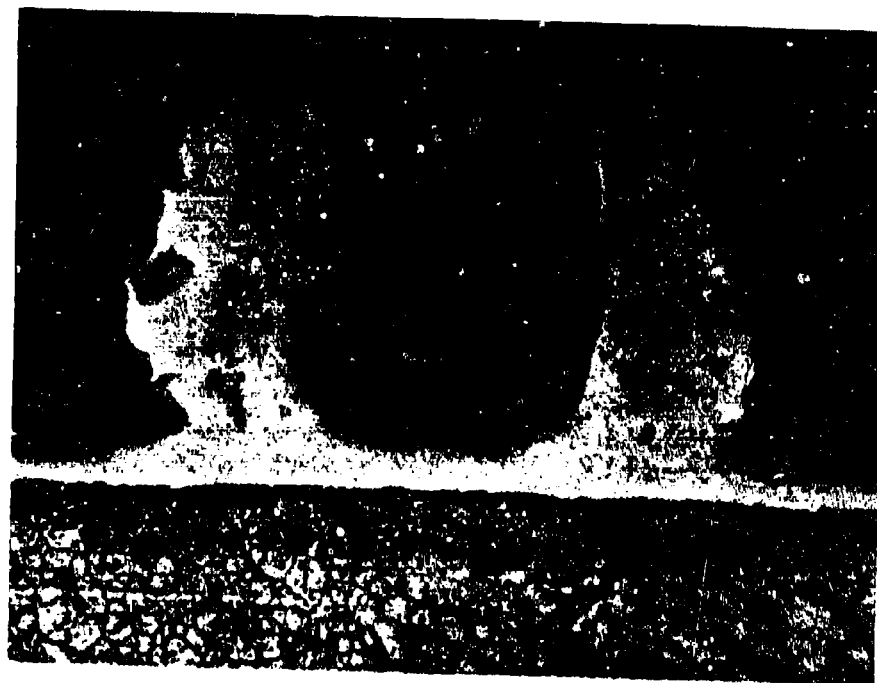
Figure 22. Core-Face Sheet Joint: Section Taken Near the Core Nodal Point (75X) - Oxalic Electroetch

and oscillated over the panel which was immersed in water. The head was traversed so that the focused ultrasound beam covered the panel in 0.016 inch increments through a 4.5 inch water column.

A Model 424B Immerscope was used to monitor the transducer power. A Model 1047 Ultragraph powered by a Sperry Sonafax Source provided the gating and printing circuitry. An Alden facsimile recorder was used to print the inspection results. The results of this inspection showed minimum voids for all panels inspection.

The focused transducer technique is extremely sensitive and is considered a reliable method of non-destructive testing the minimum fillet, high temperature honeycomb structure. The high sensitivity, however, produces problems associated with flatness. It has been established that a 0.010 inch change from the focus point of the transducer (that is, 4.5 ±.010 inch) causes enough variation in the printing signal that the instrument must be re-adjusted. The fascimiles of the 3/8 inch panels were of poorer quality than the 3/4 inch panels because of the flatness variation. The warpage of the 3/8 inch panels was excessive relative to this requirement and many adjustments were required to obtain satisfactory results. By adapting a follower to automatically adjust the transducer height over a curved panel, extremely sensitive quality inspections may be made.

(4) Visual Inspection

The diffused pattern of the core skin bond is easily visible. This pattern has proven in the past to be a reliable indication of the bond. The ultrasonic traces correspond directly to the diffused pattern, these observations thus serving as a secondary substantiation of the bond inspection results.

The cleanliness of the panel interior was excellent on the panels cut for metallurgical evaluation. There was no indication of oxide or contamination of any kind. The surfaces were similar to hydrogen bright annealed foil.

APPENDIX II

SPECTRAL NORMAL EMITTANCE MEASUREMENTS

The instrument used in making spectral emittance measurements on the L-605 specimens was a Perkin-Elmer Model 13-U Spectrophotometer with a Model 205 Diffuse Reflectance-Emittance Attachment. The L-605 specimens, in the form of 1 inch diameter disks were placed in the emission sample holder shown in Figure 23. The specimen temperature was adjusted until it was equal to that of the hohlraum cavity which served as the blackbody reference. Automatic controllers were utilized in maintaining the specimen and the reference cavity at the same temperature (within about ±1 percent). The sample holder, hohlraum cavity and transfer optics required to bring the two beams into the Model 13-U Spectrophotometer are shown in Figure 23. The specimen and reference beam path lengths through the transfer optics are equal thus cancelling effects of atmospheric absorption.

In the double-beam recording spectrophotometer the specimen and reference beams are chopped mechanically, sent through a wavelength scanning prism of sodium chloride, then alternately sensed with a thermocouple detector while the scanning is run over the spectral range from 1 to 15μ . These signals are combined electronically; the ratio being the spectral normal emittance which was plotted on a Leeds and Northrop Speedomax G Recorder.

Over the temperature range from 480 to 1400°F, the hohlraum can be maintained within ±1 percent of the temperature of the specimen thus giving an overall accuracy in emittance of approximately ±5 percent. The unit was calibrated with reference standards of platinum (low emittance), oxidized Kanthal (moderate emittance) and oxidized Inconel (high emittance) from the National Bureau of Standards (Reference 24). To further reduce potential errors in the spectral emittance data on the L-605 specimens due to small temperature and optical path lengths differences, data was obtained concurrently on the moderate emittance oxidized Kanthal reference standard. The L-605 data was reduced relative to the reference standard curve.

Results of the measurements are given in Figures 10 and 24. The various specimens were soaked in an air environment muffle furnace at the temperatures indicated in Figure 24. The extent of the soak period was such that the spectral emittance data was stable with time. The 525°F and 1050°F curves are typical of a metallic material. Slight oxidation is evidenced in the 1050°F curve. The curves at temperatures between 1250°F and 2025°F are typical of an oxide material. Visual examination of the specimens indicated that above 1200°F a stable oxide film had formed. At the highest temperatures the oxide coating was thick and quite coarse.

The vacuum environment curve shown in Figure 10 was obtained on a specimen after the vacuum conductivity run to 2010°F. In Figure 10 this curve is compared with two air environment curves from Figure 1. Some oxidation of the L-605 occurred in the high temperature vacuum test, however, the specimens still retained a metallic luster.
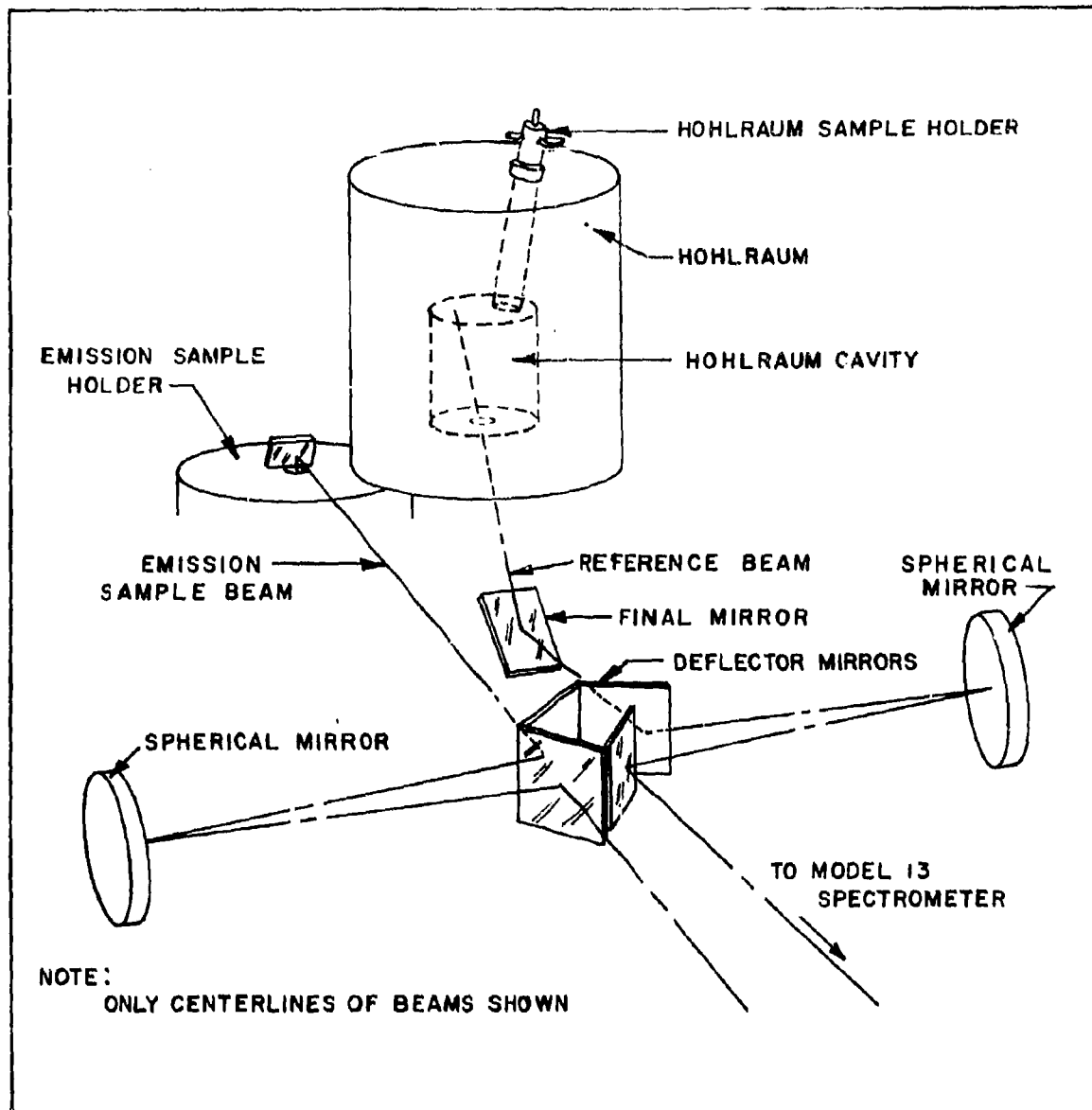
Figure 23.   Optical Arrangement for Spectral Normal Emittance Measurements
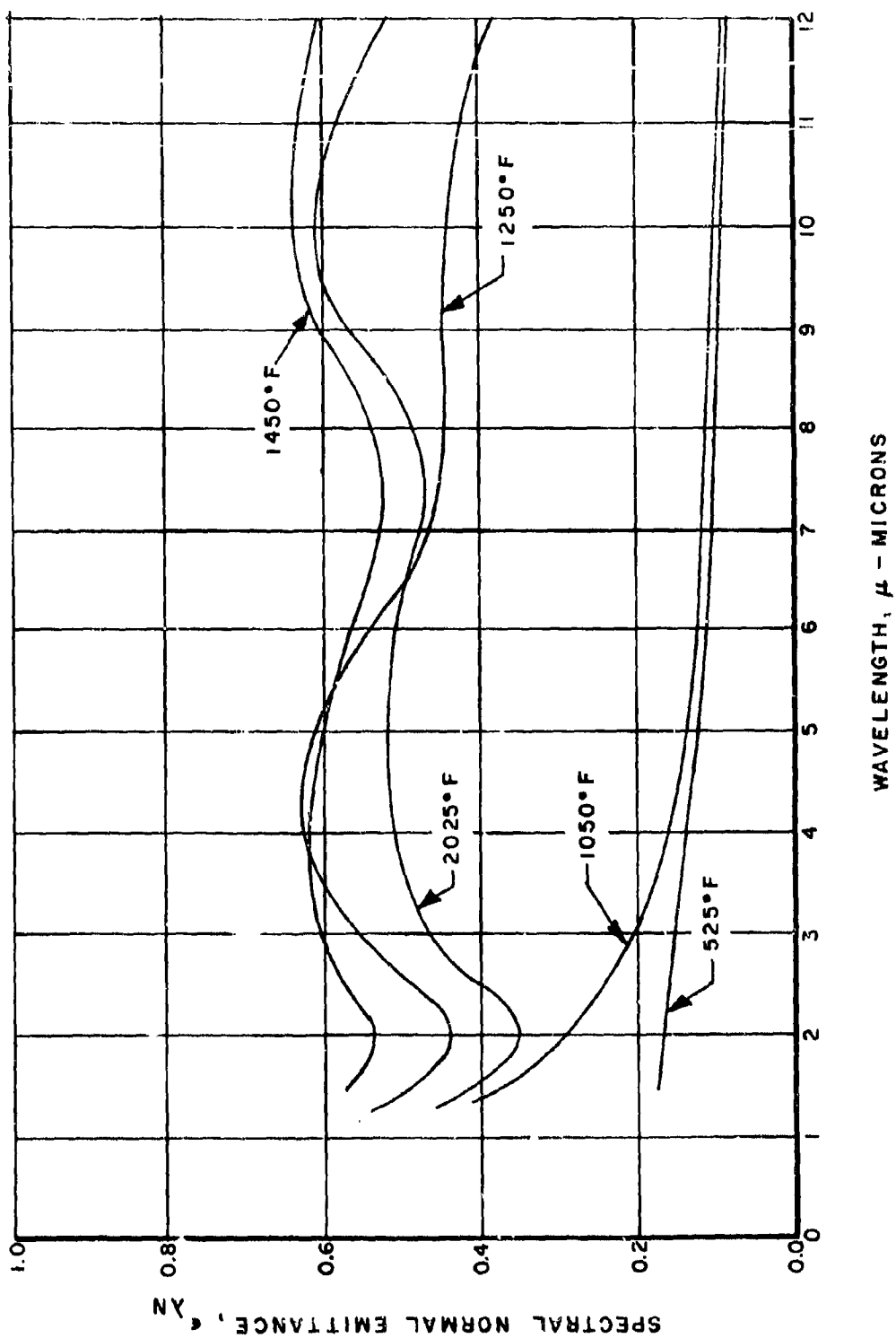
Figure 24. Spectral Normal Emittance of L-605 Cobalt Alloy as a Function of Temperature in Air Environment

APPENDIX III

TEMPERATURE GRADIENT STUDIES WITH
CYLINDERS SIMULATING HONEYCOMB CELLS

Since the analysis described earlier approximates the honeycomb cells as right circular cylinders, it was desirable to establish whether the analytically predicted gradients were of the same form as those observed experimentally.

The honeycomb panels used in the thermal conductance tests could not be instrumented to obtain axial temperature gradient in the core cells. To provide an experimental check of the predictions, fairly large, right circular cylinders of seamless stainless steel were constructed with length to diameter ratios of $1/d = 1.0$ and $1/d = 10.0$. The cylinders were instrumented axially with thermocouples and were coated on the inside surface with cobalt oxide to give a surface which was diffuse and which had an emittance of very nearly 1.0. Copper plates were silver soldered to one end of the cylinders, stainless steel plates being welded to the other. These plates assured good thermal contact between the heat sink, adjacent to the copper plate and the heat source, adjacent to the steel plate. The cylinder with $1/d = 1.0$ is shown in place in Figure 25. The lateral surfaces of the specimens were insulated heavily and a compressive load was applied to improve contact between the specimen and the heat sink and the heat source.

The results of the tests with the two cylinder geometries are summarized in Figure 15, page 30. The insert in the Figure gives the axial gradients which are predicted analytically with $\epsilon = 1.0$ for the two length to diameter ratios. For fairly small overall axial temperature drops across the panel as encountered in the honeycomb specimen testing the thermal conductivity of the metallic alloy changes very little and thus if only solid conduction were present, the temperature distribution down the walls would be nearly linear. The influence of radiation interchange is discussed in the main body of the report.

46
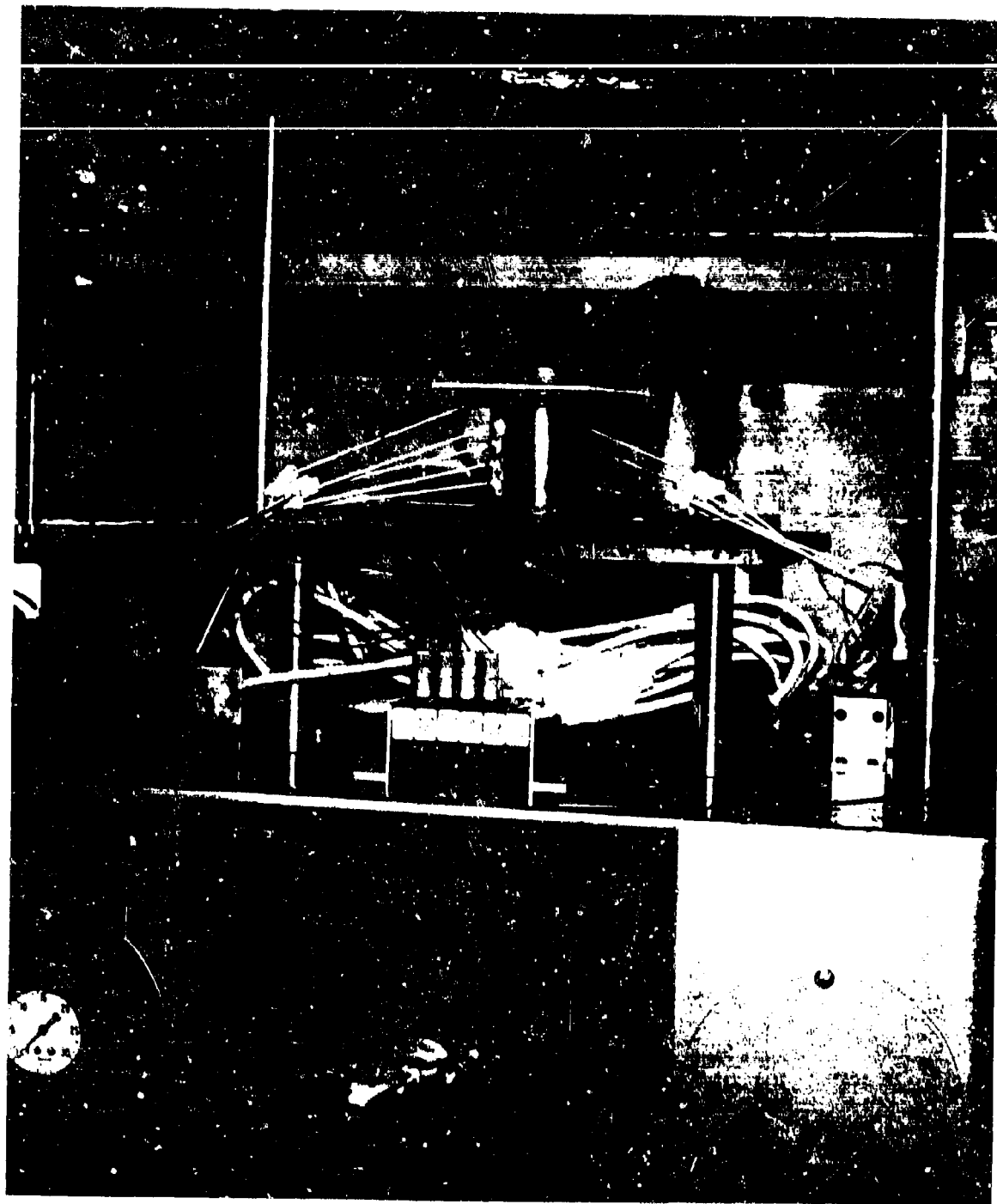
Figure 26. Cylindrical Specimen (l/d = 1.0) Used in Axial Temperature
Gradient Measurements

APPENDIX IV

TABULAR EXPERIMENTAL DATA

The following Table is a tabulation of the experimental thermal conductance data presented graphically in Figures 7 through 9.

TABLE V

EXPERIMENTAL THERMAL CONDUCTANCE DATA

Mean Panel Temperature, °F	Specimen ΔT, °F	Specimen Heat Flux, BTU/hr-ft^2	Thermal Conductance, BTU/hr-ft^2-°F
Panel #1A (Bottom, Test #3)			
Environment: Vac: 1×10^{-4} m Hg			
749	63	121	1.92
772	63	123	1.94
807	68	122	1.80
821	66	122	1.86
1210	71	304	4.28
1204	67	318	4.75
1207	68	311	4.55
1587	75	935	12.52
1600	72	934	12.97
1619	70	897	12.85
1408	53	294	5.53
1951	67	1258	18.8
Panel #1B (Top, Test #3)			
Environment: Vac: 1×10^{-4}			
756	54	76	1.42
777	55	75	1.36
812	58	76	1.29
832	66	75	1.14
1225	62	218	3.56
1218	58	244	4.18
1222	60	241	4.05
1600	70	740	10.60
1612	68	741	10.70
1631	67	723	10.82
1421	50	229	4.53
1976	67	1012.0	15.0

TABLE IV (CONT'D)

Panel #1A (Bottom, Test #3)			
Environment: Air: Atmospheric Pressure			
512	162	410	2.52
504	158	405	2.56
948	183	1140	6.23
992	181	1142	6.30
1002	174	1138	6.53
1499	140	2330	16.8
1524	133	2310	17.4
1546	122	2210	18.3
1501	127	2320	18.3
1893	115	3240	28.2
Panel #1B (Top, Test #3)			
Environment: Air: Atmospheric Pressure			
514	161	450	2.79
506	160	455	2.85
976	188	1215	6.44
984	187	1213	6.48
999	183	1217	6.68
1486	140	2380	17.05
1511	133	2400	18.0
1536	123	2260	18.3
1494	126	2390	19.8
1878	119	3200	26.8
Panel #2A (Bottom, Test #4)			
Environment: Vac: 5×10^{-5} torr			
746	42	167	3.95
652	37	201	5.46
696	37	187	5.10
1246	57	672	11.80
1636	65	1237	18.9
1643	65	1231	19.05
1950	78	2080	26.5
1966	78	2082	26.8
Panel #2B (Top, Test #4)			
Environment: Vac: 5×10^{-5} torr			
699	51	202	3.95
636	30	162	5.44
659	36	182	5.10
1166	69	816	11.75
1608	63	1188	18.90
1610	63	1194	19.00
1859	88	2320	26.25
1880	86	2318	26.80

AFML-TR-65-233

TABLE IV (CONT'D)

Panel #2A (Bottom, Test 4)			
Environment: Air: Atmospheric Pressure			
540	151	1080	7.18
888	175	2065	11.85
904	177	2065	11.67
1445	123	3480	28.40
1461	122	3480	28.60
1955	93	4600	49.60
1960	92	4600	49.80
1979	89	4530	51.30

Panel #2B (Top, Test 4)			
Environment: Air: Atmospheric Pressure			
497	138	780	5.63
817	181	1520	8.43
832	185	1520	8.23
1374	122	2460	20.20
1390	121	2460	20.36
1895	94	3270	34.70
1903	94	3270	35.00
1914	93	3290	35.30

Panel #3A (Top, Test #2)			
Environment: Air: Atmospheric Pressure			
491	81	579	7.16
845	101	880	8.70
1268	55.6	1290	23.20
1271	56	1280	22.90
1928	51	2430	47 70
1928	48	2420	50.50

Panel #3B (Bottom, Test #2)			
Environment: Air: Atmospheric Pressure			
493	96	691	7.2
862	117	1040	8.9
1291	69	1505	21.8
1295	69.5	1515	21.8
1971	66	3130	47.5
1963	65.5	3140	48.0

50

TABLE IV (CONT'D)

Panel #3B (Bottom, Test #2)			
Environment: Vacuum: 4.0×10^{-4} torr			
925	31.0	263	8.4
974	27.0	270	10.0
1557	35.5	1480	41.7
1558	35.0	1485	42.5
1489	38.0	1470	38.7
1974	54.0	3080	57.0
1965	54.0	3050	56.6
1963	55.0	2950	53.7

Panel #4A (Top, Test #1)			
Environment: Vacuum: 4.0×10^{-4} torr			
904	57	553	9.7
905	57	568	19.9
1420	65	1137	17.5
1956	71	1722	24.3
1945	67	1783	26.6

Panel #4B (Bottom, Test #1)			
Environment: Air: Atmospheric Pressure			
510	123	645	5.20
1134	69	621	9.02
1639	54	1146	21.23
1959	37	1203	32.50

SECTION VIII

REFERENCES

1. Goodyear Aircraft Corp., "Determination of Properties of Sandwich Materials Subjected to Rapid Rising Temperatures," WADC TR-59-656, (July 1960).

2. Douglas Aircraft Company, "Research on Thermomechanical Analysis of Brazed or Bonded Structural Joints," ASD TDR-63-447, (Sept 1963).

3. Ashley. H. R., "Sandwich Structure for High Temperature Vehicles," NATO, Advisory Group for Aeronautical Research and Development, Report 216, (Oct 1958).

4. King, J. P., Toy, A., Klimmek, N., "Diffusion Bonded Honeycomb Sandwich Panels," North American Aviation, Incorporated, AFML TR-64-329, (Oct 1964).

5. Krusos, J. N., Hunter, W. B., Glemza, C. J., et.al., Aeronca Manufacturing Co., "High Temperature Composite Structures," Interim ASD TR-7-845 (V), (Dec 1962).

6. Middendorp, H. J., "Materials and Processes for X-20 (Dyna-Soar)," SEG-TDR-64-20, (June 1964).

7. McCown, J. W., Wilks, G. R., Gagola, L. J., Norton, A., Schwartz, M., Martin Marietta Corp., "Manufacturing Methods and Design Procedures of Brazed Refractory Metal Honeycomb Sandwich Panels," ASD-TDR-63-767, (Sept 1963).

8. Freedman, A. H., Stone, L. H., Mikus, E. B., Northrop Corporation, "Tantalum and Molybdenum Brazing Techniques," ML-TDR-64-270, (Sept 1964).

9. "Honeycombs Bid for High Temperature Use," Chemical and Engineering News, 40, p44, (July 1962).

10. Stahman, J. A., "Development of a Ceramic Filled Honeycomb Structure for Use as an Uncooled Nozzle Extension." North American Aviation Report to NASA, (Oct 1961).

11. Vogan, J. W., Trumbull, J. L., "'Metal-Ceramic Structural Composite Materials," Boeing Company, ML-TDR-64-83, (June 1964).

12. Sparrell, J. K., Coumou, K. G., Plunkett, J. D., "An Instrument for Measuring the Thermal Conductance of High-Temperature Structural Materials," ASD-TDR-63-359, (Sept 1963).

13. Hilsenrath, J., et.al., Tables of Thermal Properties of Gases, NBS Circular 564, (Nov 1955).

14. Dunkle, R. V., "Emissivity and Inter-Reflection Relationships for Infinite Parallel Specular Surfaces," Proc Sym Thermal Radiation in Solids, Vol. 1, No. 4, (March 1964).

15. Swann, R. T., "Heat Transfer and Thermal Stresses in Sandwich Panels," NASA TN 4349, (Sept 1958).

16. Hottel, H. C., "Radiant-Heat Transmission," Chapter 4, Heat Transmission, W. H. McAdams, McGraw-Hill Book Company, Inc., New York, New York, (1954).

REFERENCES (Continued)

17. Bird, R. B., Stewart, W. E., Lightfoot. E. N., Transport Phenomena, John Wiley & Sons, Inc., New York, New York, (1962).

18. Swann, R. T., "Calculated Effective Thermal Conductivities of Honeycomb Sandwich Panels," NASA TN D-171, (Dec 1959).

19. Meghreblian, R. V., "Radiation Exchange Between Two Flat Surfaces Separated by an Absorbing Gas," Jet Propulsion Laboratory Technical Report No. 32-197, (April 1962).

20. Cohen, E. S., Hottel, H. C., "Heat Exchange in a Gas-Filled Enclosure." A.D. No. 138820, (1955).

21. Ishimoto, J., Kaysen, H., "Thermal Studies of Honeycomb Sandwich Structures Exposed to Transient External Heating-Intercell Radiation," WADC TN 57-243, (January 1958).

22. Kendall, P. J., Gonzalez, J. L, "An Analytical Model for Predicting Thermal Response in Honeycomb Sandwich Panels," AIAA Paper No. 64-258, (July 1964).

23. Solar Division of International Harvester Company, "Development of High Temperature Radiant Gas Brazing Method for Honeycomb Panels," ASD-TDR-61-7-661, (May 1961).

24. Harrison, W. N., Richmond, J. C., Shorten, F. J., Joseph, H. M., "Standardization of Thermal Emittance Measurements," National Bureau of Standards, WADC-TR-59-510, Part IV, (November 1963).

DOCUMENT CONTROL DATA - R&D

(Security classification of title, body of abstract and indexing annotation must be entered when the overall report is classified)

1. ORIGINATING ACTIVITY (Corporate author)	2a. REPORT SECURITY CLASSIFICATION
Materials Engineering Branch Materials Applications Div. Air Force Materials Laboratory	Unclassified
	2b. GROUP

3. REPORT TITLE

HEAT TRANSFER IN STRUCTURAL HONEYCOMB COMPOSITES AT HIGH TEMPERATURES

4. DESCRIPTIVE NOTES (Type of report and inclusive dates)

December 1963 to December 1964

5. AUTHOR(S) (Last name, first name, initial)

Minges, M. L.

6. REPORT DATE	7a. TOTAL NO. OF PAGES	7b. NO. OF REFS
October 1965	61	24

8a. CONTRACT OR GRANT NO.	9a. ORIGINATOR'S REPORT NUMBER(S)
b. PROJECT NO. 7381	AFML-TR-65-233
c. Task No. 738106	9b. OTHER REPORT NO(S) (Any other numbers that may be assigned this report)
d.	

10. AVAILABILITY/LIMITATION NOTICES

Each transmittal of this document outside the Department of Defense must have prior approval of the Air Force Materials Laboratory.

11. SUPPLEMENTARY NOTES	12. SPONSORING MILITARY ACTIVITY
	Materials Engineering Branch Materials Applications Div. Air Force Materials Laboratory, WPAFB,Ohio

13. ABSTRACT

The use of superalloy and refractory alloy honeycomb composites for heat shield and structural components in re-entry vehicle applications is outlined followed by a detailed comparison between experimentally measured and analytically predicted thermal conductance values on superalloy honeycomb composites.

The experimental thermal conductance determinations on L-605 cobalt alloy panels of variable geometry were made in high vacuum and air environments using a high temperature absolute thermal conductivity apparatus. Measurements were made over the range from 500° to 2000°F maintaining the temperature drop across the specimens below 200°F. Average precision of the results was ±7 percent while the accuracy was established to be ±10 percent based on initial calibration. The thermal conductances in air environment were between 60 and 100 percent above comparable values for the panels tested under vacuum conditions. Analysis of the results indicated that gaseous conduction and convection accounted for only a small fraction of the difference, the main effect being a large increase in the radiative contribution produced by increased emittance of the alloy through surface oxidation. Extensive spectral emittance measurements were made and then integrated to provide input data on temperature dependent total emittance to allow quantitative assessment of these radiative contributions.

Analytically predicted thermal conductances were based on a semi-empirical approach suggested by Swann which accounts explicitly for variations in panel geometry, panel temperature drop and materials properties (emittance and metallic thermal conductivity). Agreement with the experimental results was within a few percent at the highest test temperatures for both the vacuum and air environment conditions. At lower temperatures in air

DD FORM 1473 *1 JAN 64*

14.		LINK A		LINK B		LINK C	
KEY WORDS		ROLE	WT	ROLE	WT	ROLE	WT

INSTRUCTIONS

1. **ORIGINATING ACTIVITY:** Enter the name and address of the contractor, subcontractor, grantee, Department of Defense activity or other organization (*corporate author*) issuing the report.

2a. **REPORT SECURITY CLASSIFICATION:** Enter the overall security classification of the report. Indicate whether "Restricted Data" is included. Marking is to be in accordance with appropriate security regulations.

2b. **GROUP:** Automatic downgrading is specified in DoD Directive 5200.10 and Armed Forces Industrial Manual. Enter the group number. Also, when applicable, show that optional markings have been used for Group 3 and Group 4 as authorized.

3. **REPORT TITLE:** Enter the complete report title in all capital letters. Titles in all cases should be unclassified. If a meaningful title cannot be selected without classification, show title classification in all capitals in parenthesis immediately following the title.

4. **DESCRIPTIVE NOTES:** If appropriate, enter the type of report, e.g., interim, progress, summary, annual, or final. Give the inclusive dates when a specific reporting period is covered.

5. **AUTHOR(S):** Enter the name(s) of author(s) as shown on or in the report. Enter last name, first name, middle initial. If military, show rank and branch of service. The name of the principal author is an absolute minimum requirement.

6. **REPORT DATE:** Enter the date of the report as day, month, year; or month, year. If more than one date appears on the report, use date of publication.

7a. **TOTAL NUMBER OF PAGES:** The total page count should follow normal pagination procedures, i.e., enter the number of pages containing information.

7b. **NUMBER OF REFERENCES:** Enter the total number of references cited in the report.

8a. **CONTRACT OR GRANT NUMBER:** If appropriate, enter the applicable number of the contract or grant under which the report was written.

8b, 8c, & 8d. **PROJECT NUMBER:** Enter the appropriate military department identification, such as project number, subproject number, system numbers, task number, etc.

9a. **ORIGINATOR'S REPORT NUMBER(S):** Enter the official report number by which the document will be identified and controlled by the originating activity. This number must be unique to this report.

9b. **OTHER REPORT NUMBER(S):** If the report has been assigned any other report numbers (either by the originator or by the sponsor), also enter this number(s).

10. **AVAILABILITY/LIMITATION NOTICES:** Enter any limitations on further dissemination of the report, other than those imposed by security classification, using standard statements such as:

(1) "Qualified requesters may obtain copies of this report from DDC."

(2) "Foreign announcement and dissemination of this report by DDC is not authorized."

(3) "U. S. Government agencies may obtain copies of this report directly from DDC. Other qualified DDC users shall request through

_____ ."

(4) "U. S. military agencies may obtain copies of this report directly from DDC. Other qualified users shall request through

_____ ."

(5) "All distribution of this report is controlled. Qualified DDC users shall request through

_____ ."

If the report has been furnished to the Office of Technical Services, Department of Commerce, for sale to the public, indicate this fact and enter the price, if known.

11. **SUPPLEMENTARY NOTES:** Use for additional explanatory notes.

12. **SPONSORING MILITARY ACTIVITY:** Enter the name of the departmental project office or laboratory sponsoring (*paying for*) the research and development. Include address.

13. **ABSTRACT:** Enter an abstract giving a brief and factual summary of the document indicative of the report, even though it may also appear elsewhere in the body of the technical report. If additional space is required, a continuation sheet shall be attached.

It is highly desirable that the abstract of classified reports be unclassified. Each paragraph of the abstract shall end with an indication of the military security classification of the information in the paragraph, represented as (TS), (S), (C), or (U).

There is no limitation on the length of the abstract. However, the suggested length is from 150 to 225 words.

14. **KEY WORDS:** Key words are technically meaningful terms or short phrases that characterize a report and may be used as index entries for cataloging the report. Key words must be selected so that no security classification is required. Identifiers, such as equipment model designation, trade name, military project code name, geographic location, may be used as key words but will be followed by an indication of technical context. The assignment of links, rules, and weights is optional.

ABSTRACT (Continued)

environment the agreement was not as good, the predicted values averaging about 15 percent below the experimental data. The overall agreement between predicted and measured conductances measured in vacuum was within about 10 percent which is particularly significant because errors here in the approximated radiation interchange factors would lead to the largest errors in predicted conductance due to high reflectivity and specularity of the honeycomb cells. As a result of this experimental substantiation over a wide variation in dependent parameters it is concluded that the prediction procedure is generally useful for most engineering applications in estimating the thermal conductance of metallic honeycomb composites at high temperatures.

SUPPLEMENTARY

INFORMATION

DEPARTMENT OF THE NAVY
U. S. NAVAL PERSONNEL RESEARCH ACTIVITY
SAN DIEGO, CALIFORNIA 92152

IN REPLY REFER TO:
323:vjr
PF 016020203
Ser **801**

1 3 SEP 1966

AIR MAIL

From: Officer in Charge
To: Distribution List

Subj: Research Memorandum; pen and ink change to

Ref: (a) Automation of Operational Sequence Analysis and the
          Development of Materials for Shipboard Training of Navy
          Operator/Technicians, U. S. Naval Personnel Research
          Activity, San Diego, California SRM 66-41, June 1966

1. It is requested that the following pen and ink change be made in the
fourth line of the first paragraph on page 8 of reference (a):

Delete   "Brooks (3)"

Insert   "Kurke (11)"

G. W. WATSON